博　士　論　文

Studies on Performance Enhancement of Electric Double-Layer Capacitors Using Organic Electrolyte Solutions

有機電解液を用いた電気二重層キャパシタの高性能化に関する研究

平成 28 年 3 月

Tokita Masahiro

鴇田　真広

山口大学大学院 理工学研究科

物質工学系専攻

Contents

List of Tables

List of Figures

Chapter 1.

General Introduction

Abstract

Electric double layer capacitor (EDLC) is rechargeable electrical energy storage devices based on the capacitance of electric double layer without charge transfer reaction. Its energy storage mechanism leads to attractive properties of EDLC for the energy storage device. However, specific energy or energy density of EDLC is generally much lower than those of rechargeable batteries. In order to increase the storable electric energy, enhancing the specific capacitance and/or extending the operation cell voltage are practically efficient to realize higher-performance EDLCs.

In this work, to increase the energy density (or specific energy) of EDLC, carbon materials with controlled nano-structures have been prepared, in which efficient capacitance enhancement would be expected, and the degradation phenomena under the high-voltage cycling were examined from the viewpoints of both contributions of nano-structure of electrode material and the electrolyte components. Chapter 1 describes the general introduction including the motivation of the work. In Chapter 2, porous carbon with a uniform nano-structure was prepared by the organic template method, and then made composites with fibrous nano-carbons with highly conductive networks to obtain higher capacitance and power performances. In Chapter 3, influences of the surface structure of carbon material on the degradation behavior of EDLC were investigated. In Chapter 4, influences of the pore structure of high surface area carbon electrode were focused on the aging behavior of EDLC, especially on the capacitance and rate capability. And then, in Chapter 5, influences of the electrolyte solution components on the degradation behavior of EDLCs, which were examined under high-temperature and high-voltage conditions.

1. 1. Electric double-layer capacitor (EDLC)

1. 1. 1. Principle and characteristics of EDLC

Electrochemical capacitors (ECs), also known as “ultra-capacitors” or “super-capacitors”, are generally classified to electric double-layer- and pseudo-capacitors according to their charge-storage mechanisms. The former type utilizes the charge storage at so-called electric double layer formed at electrode/electrolyte interface [1-3].

With respect to the structure of the electric double-layer, some classical models have been proposed so far. Among them, so-called Helmholtz, Gouy-Chapman, and Stern models have been well known as typical ones that describe the electric double layer structure and are cited frequently. The Helmholtz double-layer model, shown in Fig. 1.1a, was designed as two parallel layers, consisting of an array of ions (cations or anions) located at vicinity of the electrode surface charged oppositely. It was the simplest model that could describe an approximate structure of the electrode/electrolyte interface [4]. On the other hand, the Gouy-Chapman model shown in Fig. 1.1b is based on the Boltzmann-Poison distribution of point charge from the electrode surface to the bulk of the electrolyte. This model has taken the consideration into macroscopic behavior of the molecules and ions in the electrolyte phase, based on a distribution function [5, 6]. Thus, it could be referred as more precise description than the former model. However, as the ions in the Gouy-Chapman model were treated as point charges, theoretical reproduction of the ionic states was rather hard to interpret the experimental results, especially for the capacitance behavior at the electrode surface. Therefore, an advanced model that combines Helmholtz and Gouy-Chapman models has been presented to describe the double-layer structure at the electrode/electrolyte interface more precisely. That is, so-called Stern model shown in Fig. 1.1c consists of a series combination of Helmholtz’s parallel double-layer structure and Gouy-Chapman’s diffuse double-layer structure [7]. The total capacitance evolved from the resulting electric double-layer, C_{Total}, is hence determined by Eq. (1.1),

$$1/C_{\mathrm{Total}} = 1/C_{\mathrm{H}} + 1/C_{\mathrm{Diff}} \qquad (1.1)$$

where C_{H} and C_{Diff} are electrostatic capacitances of Helmholtz and diffuse double-layers, respectively. This equation means that the lower capacitance of two (C_{H} and C_{Diff}) is more effective in the total capacitance. In the Stern model, therefore, the electrostatic

capacitance of the double-layer is almost determined by C_H whose value is generally much lower than that of C_{Diff} for a system containing sufficient concentration of the electrolyte.

Grahame presented a detailed model for double-layer structure in which a concept of "specific adsorption" is introduced [8]. Fig. 1.2 shows the schematic illustration of the Graham's model, in which ion solvation and the specific adsorption are included. In this model, the Helmholtz layer consists of two components, the arrays of adsorbed solvent molecule and, in some cases, specifically adsorbed ions. The locus of electric center of specifically adsorbed ions is called inner Helmholtz plane (IHP), whose distance is defined as χ_1. Solvated ions can approach the electrode surface with the distance χ_2, the locus of the centers of the closest solvated ions, called outer Helmholtz plane (OHP). The non-specifically adsorbed ions are distributed in a three-dimensional region, called diffuse double-layer, which extended from OHP to bulk of the electrolyte solution [9].

As mentioned above, the EDLC device stores the electrical charge, hence the energy, by a physical manner, electrostatic charge separation with forming electric double-layer. Such an energy storage mechanism in EDLC leads to much higher energy density than conventional capacitors as aluminum electrolytic capacitor, higher power density than typical secondary batteries as lithium-ion and nickel-metal hydride batteries, and extremely long cycle life over 100,000 times [10, 11]. Major similarities and differences in important and fundamental properties between EDLC and battery system are summarized in Table 1.1 [12].

Despite of many attractive characteristics as an energy storage device, EDLC still has disadvantages compared to the secondary (rechargeable) battery. Specific energy (Wh kg^{-1}) or energy density (Wh m^{-3}) of EDLC is generally much lower than that of a modern battery system (lithium-ion or nickel-metal hydride battery). Therefore, many researchers have focused on designing new electrode and electrolyte materials that enable higher energy density, or specific energy, of EDLC device, with keeping such other merits as high power and long durability. Thus, not only technical but also scientific aspects have been major issues to develop advanced EDLCs with higher energy density and/or higher specific energy.

1. 1. 2. Constituent materials for EDLC device

The EDLC device, which is a particular class of electrochemical capacitors, utilizes electrostatic force at the electrode/electrolyte interface as the charge storage source. Its performances depend on the properties of the interface. For example, the electrostatic capacitance, C_{es}, at given interface is generally express by Eq. (1.2),

$$C_{es} = \varepsilon \cdot \sigma \cdot A/d \qquad (1.2)$$

where ε and σ are dielectric and conducting components of the interface, respectively, and A and d are the cross section area and its distance at the interface. Therefore, it is quite important to choose properly both electrode and electrolyte materials that constitute the interface.

a) Electrode material

From the viewpoint of the formation of the electric double-layer structure that behaves ideally, the electrode should have smooth surface at an atomic level and a clean face without any other obstacles. One of the substances satisfying these conditions is mercury (Hg) surface. As it is a high electronic conductive metal, the applied potential (voltage) does not loose in the bulk of the electrode. Furthermore, the electrostatic capacitance per unit surface area is very high due to its liquid state with clean surface at an atomic level. The capacitance depends on the electrolyte composition. For example, it becomes high when the electrolyte consists of non-specific adsorption anion and its concentration is high. The Hg electrode does not react with this kind of electrolyte and have rather wide potential region where any faradaic reaction occurs, namely “polarizable”. Thus, it ideally shows the capacitance of about 200 - 300 mF m^{-2} in an aqueous electrolyte system [13].

Although a smooth surface of Hg electrode provides high electrostatic capacitance per unit surface area, it is not suitable for practical devices. For energy storage uses, higher specific energy (Wh kg^{-1}) and/or higher energy density (Wh m^{-3}) are desirable for practical EDLC devices. The electric energy stored in a capacitor device, U_{cap}, is expressed by Eq. (1.3),

$$U_{cap} = 1/2\ CV^2 \qquad (1.3)$$

where C and V are capacitance and operation voltage (potential) of the capacitor device,

respectively. Thus, sufficiently high capacitance is needed for a practical device. As already shown in Eq. (1.2), the capacitance is directly proportional to the cross-section area of the interface, or surface area of the electrode. Thus, materials having high specific surface area ($m^2\ g^{-1}$), or high roughness at an atomic level, are desirable to realize high specific capacitance ($F\ g^{-1}$) or high capacitance density ($F\ m^{-3}$) for the practical devices.

In the practical EDLC cells, carbon materials having high specific surface area, typically activated carbon (AC), have been widely used so far [14]. The attractive properties of high surface area carbons like AC for EDLC use are arisen from a unique combination of chemical and physical properties, i.e. high electronic conductivity, high specific surface area ($> 2000\ m^2\ g^{-1}$), good corrosion resistance, high temperature stability, controlled pore structure, processability and compatibility in composite materials, and relatively low cost [15]. In general terms, the first two properties are essential to construct an EDLC device with tolerable performances.

Common AC materials with high specific surface area are prepared from numerous carbon precursors and fabrication processes, as shown in Fig. 1.3. Porous structures of ACs are formed by chemical and/or physical activation of the carbonized precursors, in accordance with respective processing method [16]. The resulting porous carbon materials are characterized by the specific surface area, which is typically calculated from Brunauer-Emmett-Teller (BET) equation for gas adsorption isotherms. In general, high specific surface area of carbon material is resulted from complex inter-connected networks of internal pores. Under the IUPAC definition, pores are classified to “micropore” whose pore diameter is smaller than 2 nm, “mesopore” (between 2 and 50 nm) and “macropore” (larger than 50 nm), which are schematically shown in Fig. 1.4.

Usually, high BET surface area consists of smaller pore size distribution, typically with micropore and smaller region of mesopore structure. Since the carbons having much fraction of micropore region shows high specific surface area, it can provide high specific capacitance, as expected from Eq. (1.2). On the other hand, carbons in which the pore structures mainly consist of mesopore region show lower specific surface area, and hence lower specific capacitance than micropore-structure carbon. However, as ions in the electrolyte, playing important rolls to compensate the charge variations at the electrode surface, have some finite geometric sizes, especially in their solvated state, kinetic

behavior of ions in porous structure also affects the dynamism in the specific capacitance of the porous materials. That is, micropore structures of carbon materials tend to inhibit smooth ion-transport in the pores during the charge-discharge operation of the device. It has been considered that larger pore-size distribution in mesopore region would be beneficial to ion accessability in conventional organic electrolyte solutions [17-19]. Thus, for developing higher performance EDLCs, one should take into consideration of both high surface areas for specific capacitance and proper pore-size distribution for ion kinetics. From this point of view, proper pore structures have so far been considered, designed and developed in carbon materials for EDLC devices.

b) Electrolyte solutions for EDLCs

For EDLC devices, in general, any ionic conductor can be used as the electrolyte if no faradic current flows under their working voltage regions. The electrolytes are roughly classified by their nature into liquid and solid electrolytes. The former is further classified into solution electrolytes and molten salts including room-temperature ionic liquids. The solution electrolytes consist of aqueous and no-aqueous in which water and organic materials are utilized as the solvent, respectively.

Comparison of the characteristics of the aqueous and the non-aqueous electrolyte solutions is listed in Table 1.2. Typical aqueous electrolytes practically used are sulfuric acid and potassium hydroxide solutions. On the other hand, alkaline metal salts or quaternary onium salts of strong Lewis acids dissolved in aprotic organic solvents are commonly used as the non-aqueous electrolytes for EDLC. Such organic electrolyte systems have in general wider electrochemical windows, *ie.*, wider potential regions where no faradaic reaction occurs, than aqueous electrolytes have. The specific energy (or energy density) of EDLC, U, as already shown in eq. (1.3), is generally higher in EDLCs using organic electrolyte systems than those employing aqueous ones.

Table 1.3 lists selected physico-chemical properties of typical aprotic organic solvents, together with ionic conductivity and electrochemical stability (oxidation and reduction potential) of the solutions that dissolve tetraethylammonium tetrafluoroborate ($TEABF_4$) as the electrolytic salt in 1 mol dm^{-3} concentration. Acetonitrile (AN) is the most attractive solvent that shows extremely high ionic conductivity and wide potential window when

dissolving $TEABF_4$. Unfortunately, however, it has not been used for commercial EDLC devices in Japan because of its rather high vapor pressure under high-temperature conditions and possible toxicity of the thermally decomposed products. As the viscosity of propylene carbonate (PC) is higher than that of AN, ionic conductivity of PC dissolving $TEABF_4$ is lower than that of AN solution. Nevertheless, PC has been commonly used in commercial EDLC devices, because of its overall advantages, compared with other aprotic solvents. Some of commercial EDLC cells have used γ-butyrolactone (GBL) as an advanced solvent that provides highly durable electrolyte solutions under higher temperature conditions [20].

In Table 1.4, ionic conductivity of various electrolytic salts is compared for the systems dissolved in different organic solvents. The following properties are required for the electrolytic salts of EDLC devices; (1) high ionic conductivity: the internal resistance of the capacitor leads to energy loss during the charge-discharge cycles, (2) wide potential window: since the energy density (or specific energy) of EDLC is proportional to square of the operating cell voltage (see eq. (1.3)), electrochemically stable electrolytic salts are preferred over a wide potential range at any electrode materials used, (3) high specific capacitance: the double-layer capacitance of polarizable electrode depends on both the kinds of electrode material and electrolytic salt, (4) wide working temperature range: since the temperature characteristics of EDLC varies with the electrolyte system, it is required to satisfy the above properties from (1) to (3) over a wide temperature range [21].

Ionic liquids (ILs), also called room temperature molten salts, consist of any combination of cation and anion without solvents. While they belong to non-aqueous electrolyte systems, they have favorable safety characteristics such as flame retardant, non-flammable, non-volatile and high thermal stability. In general, ILs have high viscosity and rather low conductivity, especially it low temperature ranges. Therefore, they are practically used in parts as highly soluble electrolyte in organic solvents [22].

Polymeric solid electrolytes have also been expected as improved electrolyte systems having high safety and reliability for EDLC. Furthermore, due to good properties in the flexibility, they are expected to have lower manufacturing cost and improved overall cell capacitance per volume. However, they have still under development, because of their low electric (ionic) conductivity and compatibility with high surface-area electrode materials [23].

1. 2. Purpose of the present study

As already mentioned above, EDLC has very attractive properties as an energy storage device. That is, much higher power density and extremely longer cycle life (~100,000 cycles) than common secondary (rechargeable) batteries are practical advantages. However, specific energy (Wh kg^{-1}) or energy density (Wh m^{-3}) of EDLC is generally much lower than those of rechargeable batteries in which faradaic processes are utilized. In order to increase the storable electric energy, enhancing the specific capacitance and/or extending the operation cell voltage are practically efficient to realize higher-performance EDLCs.

a) Design of high performance carbon electrode

Typical EDLC cells are constructed with activated carbon (AC) as the main component of the electrode owing to its high specific surface area (~2000 m^2 g^{-1}). Conventional AC has wide pore size distribution over microporous, mesoporous and macroporous regions on the surface. As the AC with the pore structure mainly in a microporous region reveals high specific surface area (m^2 g^{-1}), it provides higher specific capacitance. On the other hand, the carbon mainly consisting of mesopore structure shows lower specific capacitance because of its lower specific surface area than micropore-based AC. However, mesopore-based carbon, or mesoporous carbon, is considered to have better capacitance capability toward higher charge-discharge current, because larger pore-size distribution of mesopore (between 2 and 5 nm) will contribute to the ion accessibility in conventional organic electrolyte solutions, as shown previously (1.1.2a). Thus, carbons for EDLC electrodes should have both high specific surface area (for capacitance) and reasonable pore size distribution (for ion kinetics). Tailoring the porous structures of carbon materials is therefore a major goal of the optimization of the EDLC electrode.

The most of recent work on nano-structure carbons for EDLC use has been focused on the preparation of controlled pore structure suitable to organic electrolyte solutions, typically $TEABF_4$ or triethylmethylammonium tetrafluoroborate ($TEMABF_4$) dissolved in PC or AN as 1 mol dm^{-3}, from the viewpoints of capacitance per volume, the effective surface area, and ion-accessibility at the carbon surface. One of the efficient methods is a

template-carbonization method, in which nanostructured and/or self-assembled materials are utilized as templates. The use of an anodic aluminum oxide (AAO) film as a porous template enables to produce carbon nanotube (CNT) or carbon nanorod as schematically shown in Fig. 1.5 [24]. Carbon-inverse opal (CIO) is prepared by using close-packed spheres with a diameter of 20–100 nm, i.e., so-called colloidal crystals or opals, as templates [25], whose synthesis procedure is shown in Fig. 1.6 (a). Mesoporous silica materials having 3D pore connections, such as MCM-48 and SBA-15, can be used as hard templates for the preparation of ordered mesoporous carbons (OMCs), as shown in Fig. 1.6 (b) [26]. The use of zeolite templates to synthesize 3D nano-carbons, zeolite-templated carbon (ZTC), has been attempted since as early as 1997 by several groups [27, 28], whose synthesis scheme is also shown in Fig. 1.7. Since ZTC has no meso-/macropores, it has higher particle density than CIOs and OMCs, and thus its volumetric surface area is also very high, up to 1800 m^2 cm^{-3} [29]. The gravimetric and volumetric surface areas of ZTCs are the highest among any carbon materials. Accordingly, ZTC offers superior capacity, hence energy, based on both gravimetric and volumetric values.

Advantages of templated nano-carbon materials are summarized as follows:

i) Unique, uniform, and/or ordered structure (1D, 2D, 3D, or hierarchical structures).

ii) High porosity in which guest species can be introduced.

iii) High surface area.

iv) Easy for heteroatom doping.

Each templated nano-carbon has at least one or several advantages classified above four categories, and these advantages are generally valuable for the energy storage applications. Also, due to these advantages, the templated nano-carbons can be used as model materials to scientifically understand many complicated physical/chemical phenomena of molecules/ions occurring in electrochemical energy storage media. Further, some of the templated nano-carbons or their composites with the advantages ii) and iv) can indeed exhibit better performances than conventional AC materials. In general, however, the templated nano-carbons have disadvantages of i) low productivity and ii) high production cost. In the template carbonization method, the necessary amount of template material is generally more than twice weight of the product carbon. Therefore, the templates which are not available in kilogram or ton order, such as AAO and opals,

will not be suitable for mass production. On the other hand, zeolites and mesoporous silica are industrial products and commercially available, so that they can be utilized practically. In any case, however, their prices are relatively expensive and, in addition, such expensive template materials are eventually removed by costly chemical etching using dangerous reagents such as hydrofluoric acid (HF).

In contrast, novel synthesis routes for OMC without hard templates have been proposed, which reduce the number of preparation steps as well as the cost involved in producing the resulting materials. This type of synthesis methods is based on organic–organic interactions between thermosetting polymers and thermally decomposable surfactants to form periodically ordered nanocomposites, as shown in Fig. 1.8 [30], which can produce pore structures depending on the type of carbon sources and the polymer materials [31-33].

In Chapter 2 of the present thesis, porous carbon with a uniform nano-structure was newly prepared by a simple preparation method above described. The resulting composites with fibrous nano-carbons were characterized and evaluated as EDLC electrode material with high specific capacitance and powercapability.

b) Higher operating voltage of EDLC cells

A typical EDLC cell uses AC-based electrodes with an organic electrolyte solution of alkylammonium salt, as $TEABF_4$, dissolved in PC or AN with around 1 mol dm^{-3} concentration. For such an electrode/electrolyte combination, durability of charge-discharge cycling becomes lowered when the cycles are done under higher voltage than *ca.* 2.7 V, especially under elevated temperature conditions. Such parasitic reactions as the decomposition of electrolyte or deformation of electrode have been proposed as the main causes of the degradation. The existences of moisture (water) impurity in non-aqueous electrolyte system and oxygen-containing surface functional groups are considered to promote the decomposition of the electrolyte [34-40]. That is, the EDLC performances would be significantly degraded under the high-voltage operation.

Carbonaceous materials generally have surface functional groups on the edge of

graphitic planes. The aging behavior of carbon-based EDLC, therefore, is considered to depend much on the graphitic structure, pore size distribution, and surface chemistry of the carbon material used. Unfortunately, however, the details of such influences have still remained unclear. The complexed pore structures and variety of surface of practical AC materials make it difficult to clarify the degradation process in organic electrolyte solutions. Therefore, in Chapter 3 of the present work, influences of graphitic structure of carbon electrode on the degradation behavior of EDLC are investigated using fibrous nano-carbons as a model electrode with simplified surface structure. Following Chapter 4 describes influences of the pore structure of high surface area carbon electrode on the aging behavior, especially on the capacitance and rate capability, using newly prepared porous carbon derived from α-cyclodextrin.

On the other hand, components of the organic electrolyte solutions also contribute to the degradation processes of EDLC, especially under high-temperature and high-voltage conditions. In some cases, an undesired process accumulates a polymer-like passivation film on the carbon-based electrode surface, which is considered to be a possible cause of the degradation behavior of EDLC [41-43]. Despite of numerous publications on this issue, optimizing the electrolyte composition for an advanced EDLC with higher energy and power keeping long cycle life is still under investigation. It should be necessary to understand in detail the degradation phenomena for different electrolyte compositions. Thus, in Chapter 5 of the present work, influences of the electrolyte components are investigated on the degradation behavior of EDLCs under server conditions.

The contents of the present thesis have already published or will be published in the following papers.

1. M. Egashira, M. Itoh, M. Tokita, N. Yoshimoto, and M. Morita, “Preparation and Capacitor Performance of Composites Based on Mesoporous Carbon/ Nanofibrous Carbons”, *TANSO*, **246**, pp. 6-10 (2011).
2. M. Tokita, M. Egashira, N. Yoshimoto, and M. Morita, “The Influence of Graphite Structure of Carbon Electrode on Aging Behavior of Electric Double Layer Capacitor”, *Electrochemistry*, **80**, pp. 752-754 (2012).

3. M. Tokita, M. Egashira, N. Yoshimoto, and M. Morita, “Capacitor Properties of Carbon Electrodes Derived from α-Cyclodextrin”, *Electrochemistry*, **81**, pp. 804-807 (2013).
4. M. Tokita, N. Yoshimoto, K. Fujii, and M. Morita, “Degradation Characteristics of Electric Double-layer Capacitors Consisting of High Surface Area Carbon Electrodes with Organic Electrolyte Solutions”, *submitted to Electrochim. Acta*.

a) Helmholtz model

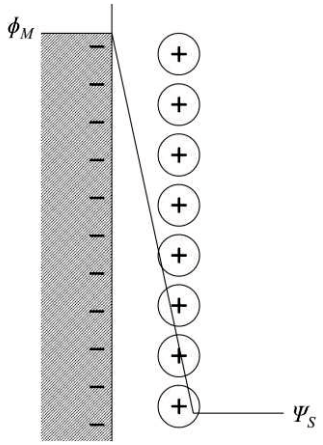

b) Gouy-Chapman model

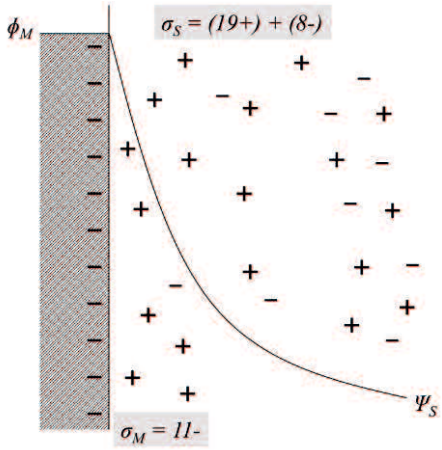

c) Stern model

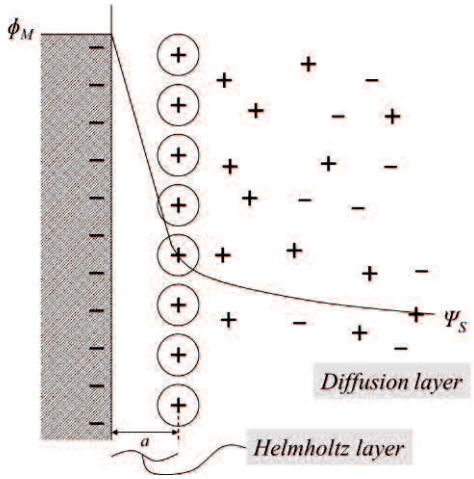

Fig. 1.1 Schematic illustration for of electric double-layer structure;
a) Helmholtz model [4], b) Gouy-Chapman model [5] and c) Stern model [6].

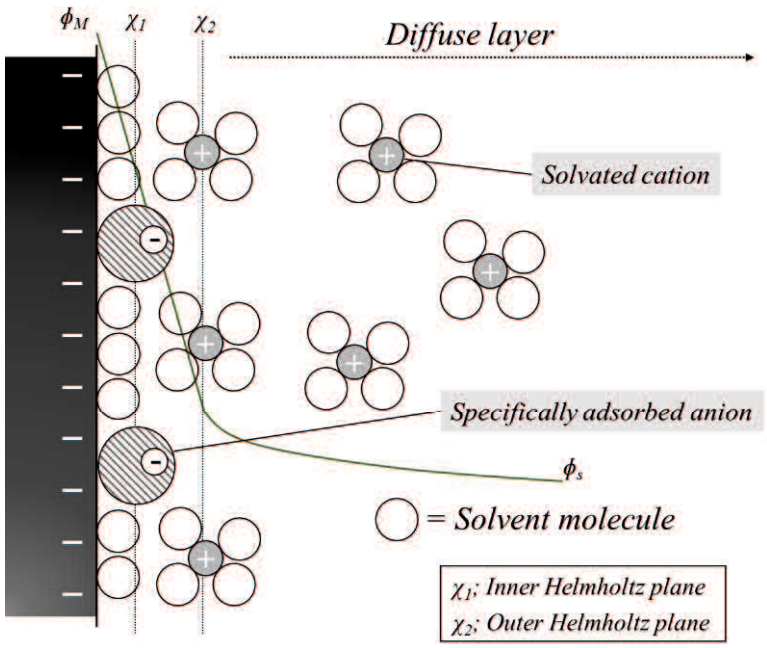

Fig. 1.2 A detailed model of electric double-layer structure proposed by Grahame [8], including the states of the solvent molecule and ions in the electrolyte.

Table 1.1 Major similarities and differences in important fundamental properties between EDLC and battery. (ref., 7)

EDLC	**Battery**
Has good intrinsic stage-of-charge indication	Does not have good intrinsic stage-of-charge indication except for Li intercalation systems
Has relatively poor energy density	Has moderate or good energy density, depending on equivalent weights and electrode potentials of active materials
Has good power density	Has relatively poorer power density, depending on kinetics
Has excellent cyclability or cycle life due to simple addition or withdrawal of charges	Has less cycle life by a factor of 1/100 ~ 1/1000 due to irreversibility of redox and phase-change processes in three dimensions
Has internal IR due to high surface area electrode material and electrolyte	Has internal IR due to electrolyte and active materials
Has little or no activation polarization	Has significant faradaic resistance
Has long lifetime except for corrosion of current collectors, etc.	Has poorer life time due to degradation or reconstruction of active materials
Electrolyte conductivity can diminish on charging due to ion adsorption	Electrolyte conductivity can decrease or increase on charging, depending on chemistry of cell reactions, e.g., with Pb-acid
Can be constructed in bipolar configuration	Can be constructed in bipolar configuration

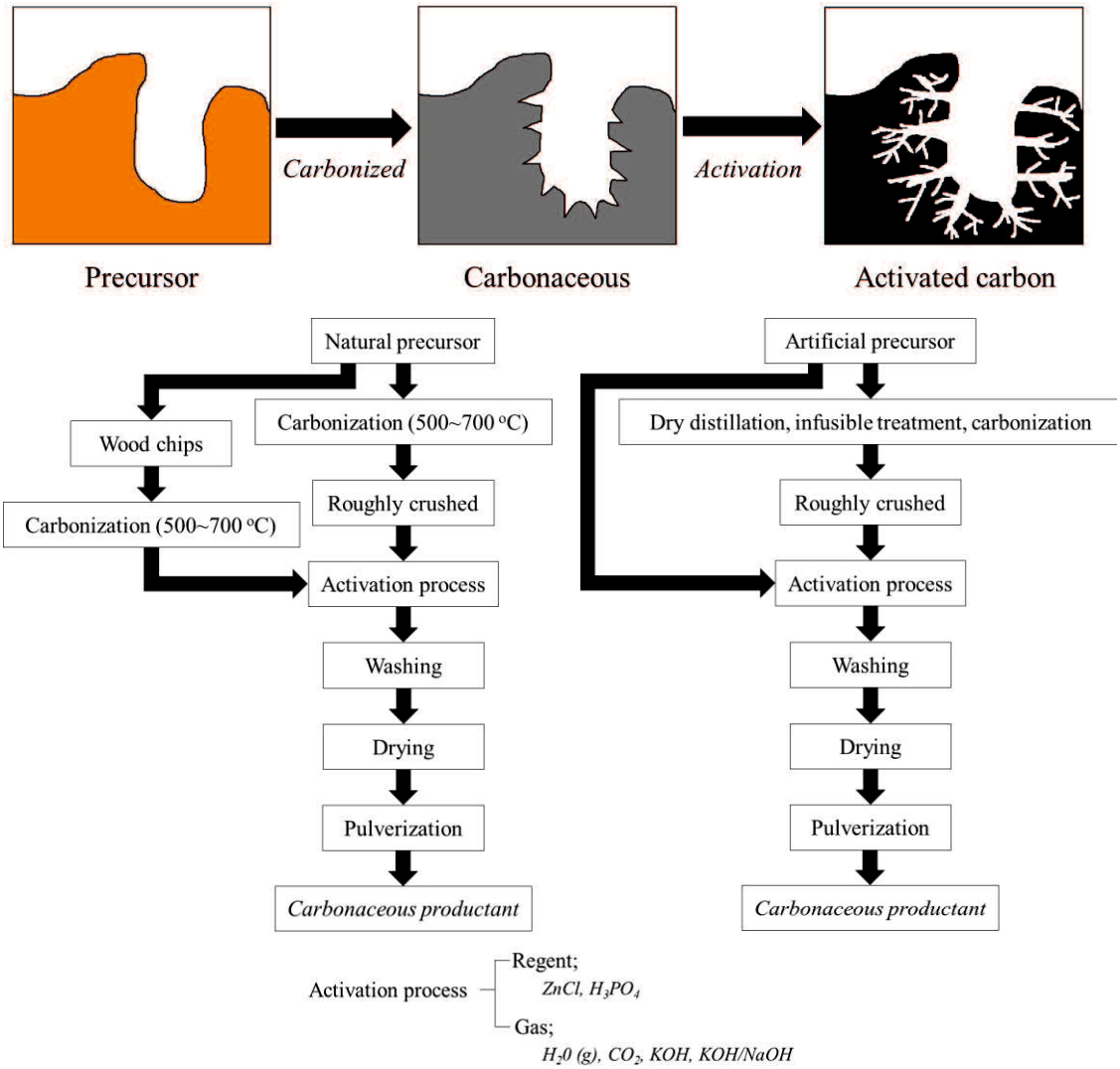

Fig. 1.3 Typical manufacturing process of activated carbon.

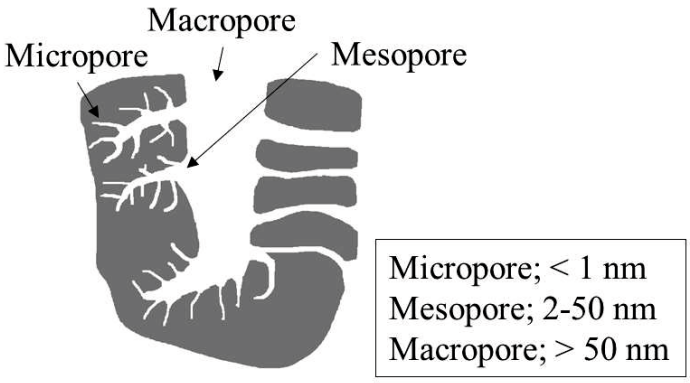

Fig. 1.4 Scheme of pore structure of activated carbon.

Table 1.2 Feather comparison of the aqueous electrolyte and non-aqueous electrolyte

Type	Advantage	Disadvantage
Aqueous	High conductivity High safety Low cost Sealed unnecessary	Low withstand voltage Narrow temperature range High corrosively
Non-aqueous	High withstand voltage Wide temperature range Low corrosively	Low conductivity Low safety High cost Sealed necessary

Table 1.3 Properties of organic solvents

Solvent	ε_r / -	η_0 / mPa s	d / g cm^{-3}	mp / °C	bp / °C	κ / mS cm^{-1}	E_{red} / V vs. SCE	E_{ox} / V vs. SCE
Ethylene carbonate (EC)	90 (40 °C)	1.9 (40 °C)	1.32 (40 °C)	36	238	17	-3.0	+3.2
Propylene carbonate (PC)	65	2.5	1.20	-49	242	13	-3.0	+3.6
γ-Butyrolactone (GBL)	39	1.7	1.12	-44	204	18	-3.0	(+5.2)
Acetonitrile (AN)	36	0.34	0.78	-44	82	56	-2.8	+3.3
Sulfolane (SL)	43 (30°C)	10.0 (30 °C)	1.26 (30 °C)	28	287	3.9	-3.1	+3.3
Dimethyl carbonate (DMC)	3.1	0.59	1.06	5	90	2.0	-3.0	+3.7
Ethyl-methyl carbonate (EMC)	3.0	0.65	1.01	-53	108	1.1	-3.0	+3.7
Diethyl carbonate (DEC)	2.8	0.75	0.97	-74	127	0.6	-3.0	+3.7

Table 1.4 Properties of electrolytic salts

Electrolyte salt	PC	GBL	AN
$LiBF_4$	3.4	7.5	18
Me_4NBF_4	2.7	2.9	10
Et_4NBF_4	13	18	56
Pr_4NBF_4	9.8	12	43
Bu_4NBF_4	7.4	9.4	32
$LiPF_6$	5.8	11	50
Me_4NPF_6	2.2*	3.7*	12*
Et_4NPF_6	12	16	55
Pr_4NPF_6	6.4*	11	42
Bu_4NPF_6	6.1	8.6	31
$LiClO_4$	5.6	11	32
Me_4ClO_4	2.9*	3.9*	7.7*
Et_4ClO_4	11	16	50
Pr_4ClO_4	6.3*	11*	35*
Bu_4ClO_4	6.0	8.1	27
$LiCF_3SO_3$	1.7	4.3	9.7
$Me_4CF_3SO_3$	9.0*	14	46
$Et_4CF_3SO_3$	11	15	42
$Pr_4CF_3SO_3$	7.8	11	31
$Bu_4CF_3SO_3$	5.7	7.4	23
$Li(CF_3SO_3)_2N$	5.1	9.4	
$Me_4(CF_3SO_3)_2N$	11		
$Et_4(CF_3SO_3)_2N$	11		

In mS cm^{-1} at 1mol dm^{-3} (*saturated concentration), 278 K

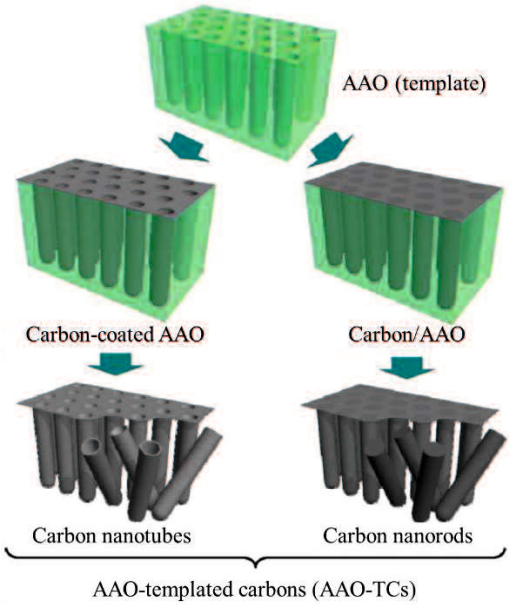

Fig. 1.5 A synthesis of AAO-templated carbons (AAO-TCs); carbon nanotubes (left) and carbon nanorods (right).

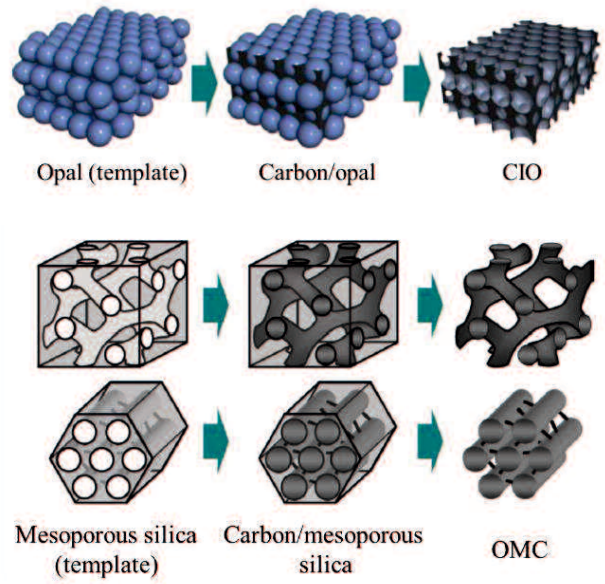

Fig. 1.6 A synthesis of (a) carbon inverse opal (CIO) and (b) two type of ordered mesoporous carbons (OMCs) from MCM-48 (upper) and SBA-15 (bottom).

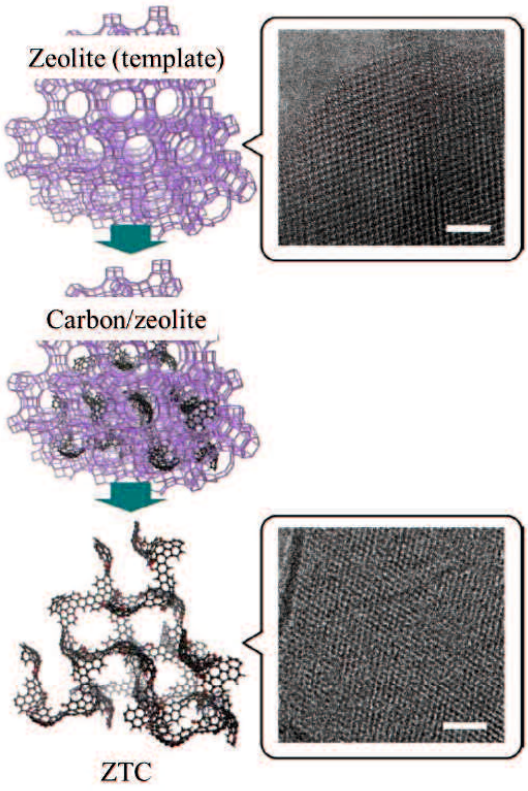

Fig. 1.7 A synthesis scheme of zeolite-templated carbon (ZTCs) together with TEM images of zeolite Y and ZTC.

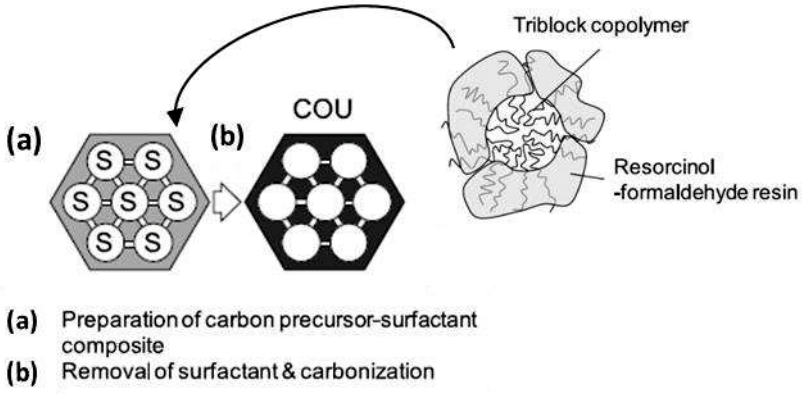

Fig. 1.8 Schematic illustration of the synthesis routes for ordered mesoporous carbons by the soft-template method.

Reference

[1] D. Qu and H. Shi, *Journal of Power Sources*, **74**, 99 (1998).

[2] E. Frackowiak and F. Béguin, *Carbon*, **39**, 937 (2001).

[3] F. Béguin, V. Presser, A. Balducci, and E. Frackowiak, *Advanced Material*, **26**, 2219 (2014).

[4] H. von Helmholtz, *Ann. Phys*., **89**, 211 (1853).

[5] G. Gouy, *Ann. Phys.,* **7**, 129 (1917).

[6] D. L. Chapman, *Phil. Mag*., **25**, 475 (1913).

[7] O. Stern, *Zeit. Electrochem.*, **30**, 508 (1924).

[8] D. C. Grahame, *Chem. Rev*., **41**, 441 (1947).

[9] J. D. Bernal and R. H. Fowler, *J. Chem. Phys*., **1**, 515 (1933).

[10] P. Simon and A.F. Burke, *Interface*, **17**, 38 (2008).

[11] M. Arulepp, L. Permann, J. Leis, A. Perkson, K, Rumma, A. Janes and E. Lust, *Journal of Power Sources*, **133**, 320 (2004).

[12] B. E. Conway, *Electrochemical Supercapacitors*, Scientific Fundamentals and Technological Applications, Kluwer Academic/Plenum Publishers, Chapter 2, New York, (1999).

[13] R. Parsons, Modern Aspects of Electrochemistry, J. O'M. Bockris and B.E. Conway, and R. White, eds., vol. 1, Chapter 4, London (1954).

[14] D. Qu and H. Shi, *Journal of Power Source*, **74**, 99 (1998).

[15] B. Kastening, M. Hahn, B, Rabanus, M. Heins and U. Felde, *Electrochimica Acta*, **42**, 2789 (1998).

[16] G. S. Miguel, G. D. Fowler and C. J. Sollars, *Carbon*, **41**, 1009 (2003).

[17] L. Wang, T. Morishita, M. Toyoda and M. Inagaki, *Electrochimica Acta*, **53**, 882 (2007).

[18] J. Chmiola, G. Yushin, R. Dash and Y. Gogotsi, Journal of Power Sources, **158**, 765, (2006).

[19] G. Gryglewicz, J. Machnikowski, E. Lorenc-Grabowska, G. Lota and E. Frackowiak, *Electrochimica Acta*, **50**, 1197 (2005).

[20] A. Yoshida, K. Nishida, S. Nonaka, S. Nomoto, M. Ikeda and S. Ikuta, Japanese Patent 9-266143, (to Matsushita Electric), 1997.

[21] F. Béguin, V. Presser, A. Balducci and E. Frackowiak, *Advanced Materials*, **26**, 2219 (2014).

[22] C. Largeot, P. L. Taberna, Y. Gogotsi and P. Simon, *Electrochemical and Solid-State Letters*, **14**, A174 (2011).

[23] P. Simon and Y. Gogotsi, *Nature Materials*, **7**, 845 (2008)

[24] T. Kyotani, *Bull. Chem. Soc. Jpn*., **79**, 1322 (2006).

[25] A.A. Zakhidov, R.H. Baughman, Z. Iqbal, C.X. Cui, I. Khayrullin, S.O. Dantas, I. Marti and V.G. Ralchenko, *Science*, **282**, 897 (1998).

[26] H.Y. Liu, K.P. Wang and H.S. Teng, *Carbon*, **43**, 559 (2005).

[27] T. Kyotani, Z.X. Ma and A. Tomita, *Carbon*, **41**, 1451 (2003).

[28] K. Matsuoka, Y. Yamagishi, T. Yamazaki, N. Setoyama, A. Tomita and T. Kyotani, *Carbon*, **43**, 876 (2005).

[29] H. Nishihara, H. Itoi, T. Kogure, P.X. Hou, H. Touhara, F. Okino and T. Kyotani, *Chem-Eur. J*., **15**, 5355 (2009).

[30] R. Ryoo, S.H. Joo, M. Kruk and M. Jaroniec, *Adv. Mater*., **13**, 677 (2001).

[31] S. Tanaka, N. Nishiyama, Y. Egashira and K. Ueyama, *Chem. Commun*., 2125 (2005).

[32] F. Zhang, Y. Meng, D. Gu, Y. Yan, C. Yu, B. Tu and D. Zhao, J. Am. Chem. Soc., **127**, 13508 (2005).

[33] Y. Meng, D. Gu, F. Zhang, Y. Shi, H. Yang, Z. Li, C. Yu, B. Tu and D. Zhao, *Angew. Chem. Int. Ed*., **44**, 7053 (2005).

[34] O. Bohlen, J. Kowal and D.U. Sauer, *J. Power Sources*, **172**, 468 (2007).

[35] P. Kurzweil and M. Chwistek, *J. Power Sources*, **176**, 555 (2008).

[36] R. Kötz, P. W. Ruch, and D. Cericola, *J. Power Sources*, **195**, 923 (2010).

[37] P. W. Ruch, D. Cericola, A. Foelske, R. Kötz, and A. Wokaun, *Electrochim. Acta*, **55**, 2352 (2010).

[38] O. Bohlen, J. Kowal, and D. U. Sauer, *J. Power Sources*, **172**, 468 (2007).

[39] O. Bohlen, J. Kowal, and D. U. Sauer, *J. Power Sources*, **173**, 626 (2007).

[40] H. Gualous, R. Gallay, G. Alcicek, B. Tala-Ighil, A. Oukaour, B. Boudart, and Ph. Makany, *Microelectron. Reliab.*, **50**, 1783 (2010).

[41] A.M. Bittner, M. Zhu, Y. Yang, H.F. Waibel, M. Konuma, U. Starke and C.J. Weber, J. Power Sources, 203, 262 (2012).

[42] P.W. Ruch, D. Cericola, A. Foelske, R. Kötz, Electrochim. Acta, 55, 2352 (2010).

[43] S. Pohlmann, B. Lobato and T.A. Centeno, *Phys. Chem*., **15**, 17287 (2013).

Chapter 2.

Preparation and Capacitor Performance of Composites Based on Mesoporous carbon /Nanofibrous Carbons

Abstract

Composites have been prepared by the carbonization of an ordered mesoporous carbon precursor coated on nano-carbon substrates for high-rate double-layer capacitor electrodes. The reproducibility of mesopore structure at 3.8 nm depends on the carbonization conditions, the loading amount of precursor, and the substrate. The specific surface area of the composite based on vapor grown carbon fiber (VGCF) reaches 250 m^2 g^{-1} and has unique pore characteristics. The test cell with the composite based on VGCF exhibited ca. 4 F g^{-1} of specific capacitance at best and maintained the capacitance under high-rate conditions. The capacitance of the test cell with the composite electrodes depends on the pore structure of the composite.

2. 1. Introduction

Electric double-layer capacitor (EDLC) has been attracted not only as back-up charge storage but as novel power source or power assist with providing high power density. Double-layer is a capacitive layer formed at electrode/electrolyte interface, thus various porous carbons with high surface area have been applied as electrode materials for this kind of device. On the use of a porous carbon in a double-layer capacitor, the pore size in the carbon electrode is limited to the extent in which ions are accessible and can form double-layer inside. Porous carbon electrodes having adequate pore size distribution may provide double-layer capacitors with high energy and power densities [1-4].

Conventional activated carbons are prepared by the partial oxidation of amorphous carbons, and thus they have broad pore size distribution from micro- to macropores. Inactive pores may only increase the materials brittleness and the electronic resistance of the activated carbon without any positive contributions. From this viewpoint, carbons having uniform mesopores have been designed for the use in the electrode. Various mesoporous carbons have been prepared for this purpose such as the carbon obtained from poly(tetrafluoroethylene) [5], activated carbons prepared with zinc chloride [6, 7], carbons from the precursors containing rare earth complexes [8], heat-treated fullerene soot [9], and the carbons prepared by 'hard template' method where carbon sources are filled in nanospaces of inorganic porous materials [10-17]. Moreover, recently those methods where some micelles in liquid phase created by a triblock copolymer surfactant are used as template have been progressed [18, 19]. These methods are elegant for obtaining porous carbons with desired pore structure, while the morphology of the carbons is limited by the one of the inorganic template.

The structure of electrode at micron or submicron level is expected to be related for the mass transfer of electrolyte concerning high-rate capability of capacitors. In addition, the electronic conductance, which is spoiled by amorphous and porous structure, is also important for the high-rate performance. For these reasons, carbon nanotube (CNT) is reported to exhibit good high-rate properties, while its specific capacitance is rather low due to its small surface area [20-25]. Such carbon materials having good conductivity, accessible pore structure and morphology, is favorable for the use in double-layer

capacitors with sufficient high-rate performance. The concept of carbon composite might be effective to take these contradict properties. In the present trial, composites of mesoporous carbon (MC) with substrates having characteristic microstructures have been prepared and evaluated for capacitor electrode. Here the resorcinol-formaldehyde (R-F) gel containing a triblock copolymer surfactant is selected as a source of MC with uniform mesopores. For the substrate, microfibrous carbons such as vapor grown carbon fiber (VGCF) and CNT are selected. At the first step the preparation condition has been optimized, and for a certain case the capacitor cell performance has been introduced here.

2. 2. Experimental

2. 2. 1. Preparation of carbon composite

VGCF (Showa Denko Co., average fiber diameter ca. 200 nm) and CNT (Nanocyl Inc.) were used as substrate nano-carbon materials. A precursor solution according to a previous report [18], prepared by dissolving 2.3 g ethanol, 0.06 ml of 5 mol dm^{-3} hydrochloric acid, 0.661 g of resolcinol, equivalent formaldehyde solution, 0.487 g of triethyl orthoacetate, and 0.378 g of triblock copolymer surfactant Pluronic F127 (BASF) into 1.74 g of distilled water, was mixed with a substrate, as the gravimetric ratio of substrate : precursor solution was set at 1 : 4 (80 wt% MC) or 1 : 9 (90 wt% MC). The mixture, with a texture of hard slurry, was cured at 90 ^{o}C during 24 h. Then the cured material was heated at 1000 ^{o}C under the flow of argon, in two-kinds of furnaces with different flow of argon as shown in Fig. 2.1: in one case the heated material was placed on the refluxing argon flow, while in the other case argon flowed through the material. The heat-treatment temperature was 1000 ^{o}C, with stepwise heating by 200 ^{o}C in 1 h. The carbon yields of the heat-treated products based on the R-F gel fraction in the precursor were within several percent. The composites are denoted by the substrate, content of precursor and the heating furnace as shown in Table 2.1.

2. 2. 2. Characterization of carbon composite

The BET surface area of the carbonaceous materials was determined from the nitrogen adsorption isotherms using a sorptometer (NOVA2000, Quanterchrome Inc.). The pore size distributions of the materials were calculated by the desorption isotherm based on BJH method. Materials for the adsorption measurement were heated at 200 ^{o}C under vacuum before the measurement. The morphology and structure of composite material was observed using a scanning electron microscope (VE-8800, Keyence Co., Japan) and a transmitted electron microscope (JEM-6020, JEOL Co., Japan).

2. 2. 3. Capacitor cell performance

The properties of a VGCF/MC composite as double-layer capacitor electrode were

estimated by using a 2-electrode test cell with Teflon body. The electrode active material was molded with 10 wt% of poly (tetrafluoroethylene) (PTFE) binder, cut into disk shape with 1.3 cm diameter, attached with platinum mesh current collector, and then assembled into a sealed cell with a round-shaped glass filter separator with 0.2 mm thick soaked by electrolyte, 1 mol dm^{-3} tetraethylammonium tetrafluoroborate ($TEABF_4$; Tomiyama Pure Chemical Co., Japan) solution in propylene carbonate (PC; Kishida Chemical Co., Japan). A cell contains ca. 0.025 g of electrode active mass (sum of both electrodes). The cell was assembled in a glove box filled with argon. As a comparison, the cell was prepared with bare CNT electrodes. The constant current charge-discharge tests were conducted for the cells under such conditions as the cut-off voltage of 0 to 2 V, and prescribed current, using a cycler (Nagano Electric Co., BTS-2003).

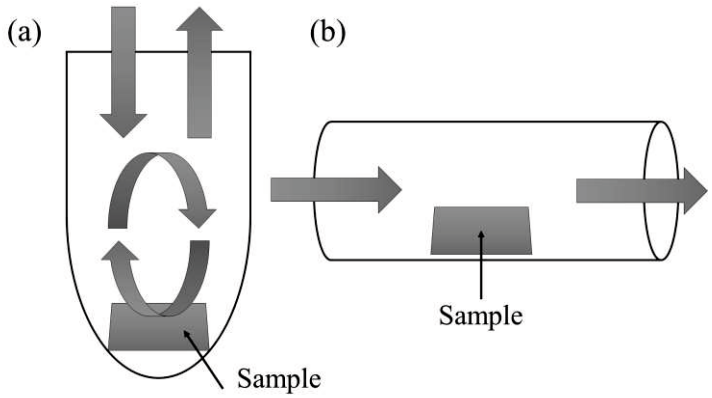

Fig. 2.1 Schematic models of furnaces and argon flow inside these furnaces. (a) reflux (b) direct flow.

Table 2.1 Specific Surface Areas (SSA) of the Mesoporous Carbon /Carbon Composites

substrate	furnace	MC precursor content [wt%]	notation	SSA [$m^2 g^{-1}$]
VGCF	(bare)		VGCF	20
	reflux	80	VGCF/MC-R80	131
		90	VGCF/MC-R90	253
	direct flow	80	VGCF/MC-D80	115
		90	VGCF/MC-D90	215
CNT	(bare)		CNT	270
	reflux	80	CNT/MC-R80	337
		90	CNT/MC-R90	373
	direct flow	80	CNT/MC-D80	280
		90	CNT-MC-D90	350

2. 3. Results and discussion

2. 3. 1. Pore structure of composites

The SEM image of the VGCF/MC-R90 composite is shown in Fig. 2.2 (a). Mainly fibrous feature of VGCF partially covered with resin-like shape is observable. The typical TEM image of the VGCF/MC composite is shown in Fig. 2.2 (b). A rod-like VGCF fibrous can be clearly observed. The MC portion is observable as amorphous feature, with round patterns of tens nanometers, attached on VGCF. Such round patterns are assumed as mesopores created by the aid of triblock copolymer in the precursor, as observed in a previous report [19]. From the SEM image in Fig. 2.2 (a), MC appears to be attached only in the part of each fiber. In contrast, the TEM image clearly shows that a fiber body is coated with MC, while the coating layer may be thinner than the observable level by SEM. It is difficult to be regarded that the mesopores are ordered as indicated in the literature, probably due to the substrate is not smooth nor uniform. The TEM image clearly indicates that the MC fraction is attached on VGCF substrate, not isolated, as expected.

Fig. 2.3 shows the typical nitrogen adsorption and desorption isotherms for the VGCF/MC composite carbons with the comparison to that for VGCF substrate. The VGCF/MC composites show II-type isotherms with increased total adsorption/desorption volumes compared with substrates. The hysteresis loop between adsorption and desorption is unclear, suggesting that the pores may be cylindrical. The specific surface areas of the VGCF/MC composite carbons prepared with various compositions and carbonization processes are summarized in Table 2.1. The specific surface area of VGCF substrate is 20 $m^2 g^{-1}$, and the surface areas of the VGCF/MC composites are significantly larger than that of VGCF, and larger by the larger amount of MC portion. From the comparison on the carbonization process, the refluxing argon flow provides larger surface area for the composite than the on-site flow system.

The pore size distribution of a carbonaceous material prepared from the MC source described in this study is shown in Fig. 2.4 (a) (HTT in the case was 1000 ^oC). The MC source provides significant pores having narrow pore size distribution around 3.8 nm. The pore size distribution of typical VGCF/MC composite is illustrated in Fig. 2.4 compared with VGCF. While VGCF shows a broad pore size distribution over 2 to 20 nm, the

VGCF/MC composites show two large peaks: a sharp one at 3.8 nm and a broad one between 5 and 30 nm. Pore volumes for both peaks in the profile of the VGCF/MC composites are larger than that for VGCF substrate, and the contribution of each peak is different by the composition and the carbonization process of the composites. The peak at 3.8 nm originates from the pore formed in the MC portion, while the one at 5 to 30 nm may be slits by the stacks of VGCF fibers covered with the MC portion or the combination of the former pores. The pore characteristics, in particular volumes of the pore with 3.8 nm diameter and their contributions to the total pore volumes, for the VGCF/MC composites are mentioned in Table 2.2. All the VGCF/MC composites prepared here exhibit larger contribution of 3.8 nm pore to the total pore volumes than VGCF. It is difficult to find any relationships between the carbonization conditions and the volume of the pore with 3.8 nm diameter. Perhaps the contribution of the 3.8 nm pore is influenced by the behavior of the surfactant in the MC source. In other words, in the cases of the VGCF/MC-R90 where the contribution of the 3.8 nm pore is small, the surfactant may cause the 'activation' of the surface of the composites. Under the direct flow condition, the contribution of the 3.8 nm pore appears to be unchanged by the composition of the precursor probably due to the renewal of heating atmosphere, while the acceleration of carbonization may create some irregular pores. It is indicated from this result that the balance of the carbonization and the evaporation of the surfactant determines the contribution of the 3.8 nm pore to the total pore volume. Among the trials of which results are summarized in Tables 2.1 and 2.2, the cases such as the VGCF/MC-R80 reproduce well the selective pore structure of the MC.

The SEM images of the CNT/MC composite are shown in Fig. 2.5. The aggregates of CNTs with secondary particles of several micrometers are observable without any signs of resin feature. Perhaps MC source is coated onto entire CNT surface. The specific surface areas and the pore characteristics in the CNT/MC composites are also included in Tables 2.1 and 2.2, and typical pore size distributions of the CNT/MC composite. The surface areas of the CNT/MC composites are at similar extent, ca. 300 m^2 g^{-1}, to the substrate. In addition, their pore size distributions are rather similar to that of CNT itself, with a small impact of the 3.8 nm pore. This result indicates that the MC portion would not provide the characteristic pore structure. The MC portion appears to cover CNT in

these composites as it does on VGCF in the VGCF/MC, because no signs of the existence of isolated MC portion, which would exhibit the narrow pore distribution on 3.8 nm, are found in the pore size distribution profile. The surface layer of the MC on CNT may be thin at insufficient extent for the formation of the pore structure, or the surfactant may be consumed by the adhesion between CNT and the MC precursor.

2. 3. 2. Capacitor performance of the cell containing VGCF/MC electrodes

The VGCF/MC composites are applied for the electrodes at the present trial because the hybridization effect is more significant in the case of the VGCF/MC. In order to clarify the influence of pore structure to the electrode properties, the CNT electrode, which has high surface area without closed pore structure, was prepared and used as comparison. Fig. 2.6 shows the constant current charge-discharge profile of capacitor cells containing (b) VGCF/MC-D90, (c) VGCF/MC-R90, and (d) VGCF/MC-R80 electrodes compared with the one containing (a) bare CNT electrodes at similar currents. All the profiles exhibit triangular shape similar to those for typical double-layer capacitors. The rate capabilities of the capacitances of the cells (normalized by the mass of the electrodes) containing CNT and the VGCF/MC electrodes are summarized in Fig. 2.7. The capacitances of all the cells are rather low compared with conventional activated carbon double-layer capacitors because of the lower surface areas (130 ~ 270 m^2 g^{-1}) of the electrodes than conventional activated carbons (1000 ~ 3000 m^2 g^{-1}). The values of cell capacitances divided by the SSA of the electrodes are around 1.8×10^{-2} F m^{-2} (approximately corresponding to 7.6 μF cm^{-2} for capacitance per electrode unit surface) except for the VGCF/MC-R90 (1.4×10^{-2} F m^{-2}; approximately corresponding to 5.6 μF cm^{-2} per electrode unit surface), which contains rather small amount of 3.8 nm mesopore. The VGCF/MC-R90 has large amount of micropores which are not available for double-layer charge-discharge process. In contrast, mesopores of 3.8 nm appear to provide capacitances similar to smooth surface of CNT. All the cells maintain their capacitances even at 2 mA cm^{-2} of current density, while the capacitances of the cells with the VGCF/MC electrodes decrease slightly at the higher current rate. The influencing factor of the rate capability is somewhat complicated including not only the electrode conductivity but the status of cell assembly. When

conventional activated carbons are used as electrode in similar configuration, the ratios of the capacitances at 1 mA cm^{-2} to 0.1 mA cm^{-2} are varied around 50 ~ 60 %. All the cells shown in Fig. 2.7 appears to exhibit improved rate capability compared with such the cases of conventional activated carbon. Therefore, the VGCF/MC composites as well as the CNT are assumed to provide good capacitance retention at high current rate. This result indicates that the capacitance provided by the 3.8 nm mesopore exhibits similar rate duration compared with the smooth surface of the CNT. Moreover, it should be noted that the composite carbons, exhibiting comparable electrode properties of the CNT, are prepared from VGCF with lower surface area substrate. It is expected that further modification of substrate and compositing procedure provides composite carbons with much improved properties for capacitor electrodes.

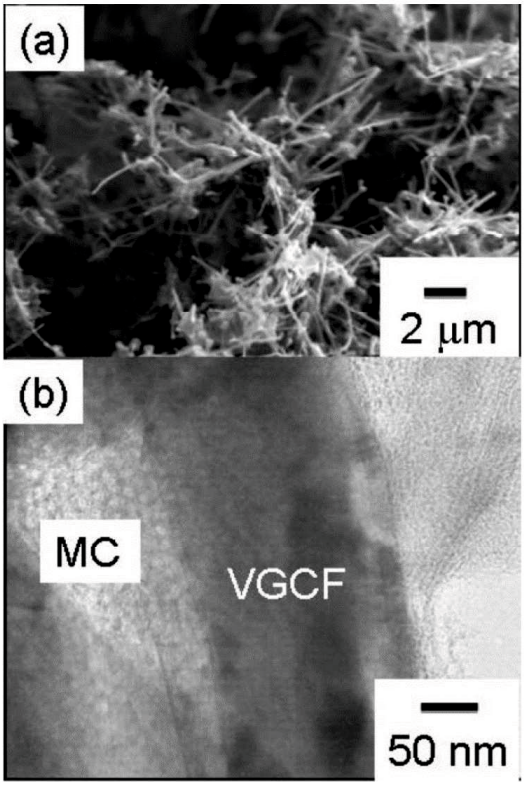

Fig. 2.2 (a) SEM and (b) TEM images of the VGCF/MC-R90 composite

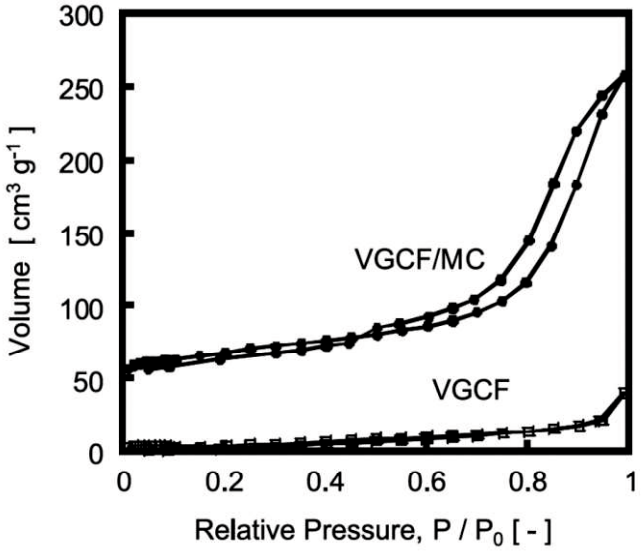

Fig. 2.3 Nitrogen adsorption/desorption isotherms of VGCF and the VGCF/MC-R90 composite.

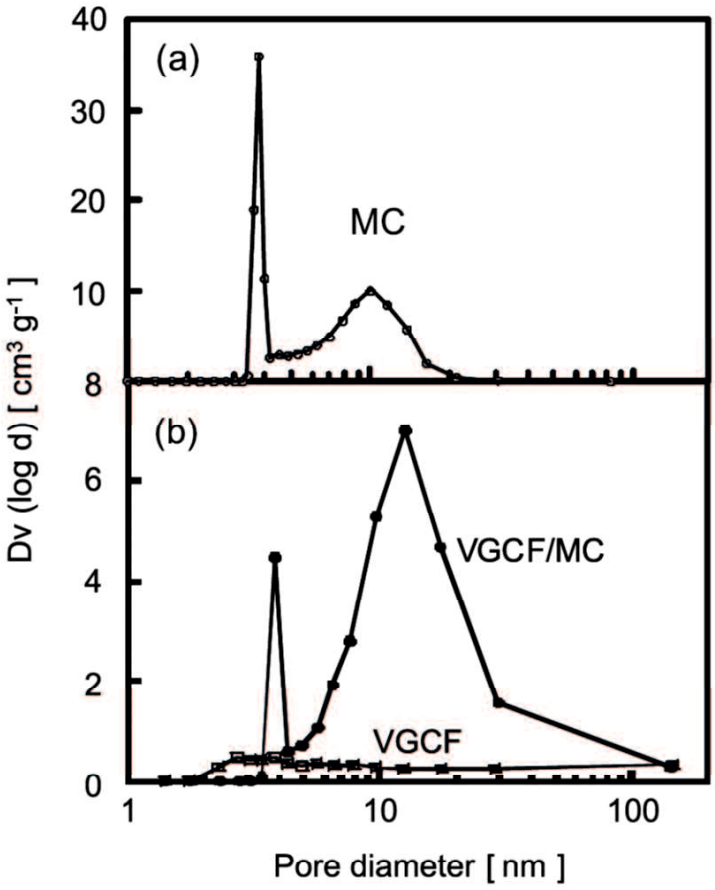

Fig. 2.4 Pore size distributions of carbons. (a) Mesoporous carbon (MC) prepared from Pluronic/R-F gel. (b) VGCF and the VGCF/MC-R90 composite.

Table 2.2 Pore characteristics of the mesoporous carbon/carbon composites

material	pore volume [$cm^3\ g^{-1}$]		contribution of 3.8 nm pore [%]
	total	3.8 nm	
VGCF	5.3	0.48	9
VGCF/MC-R80	14.1	7.4	53
VGCF/MC-R90	30.6	4.5	15
VGCF/MC-D80	14.7	4.5	31
VGCF/MC-D90	28.0	7.8	28
CNT	73.7	2.8	4
CNT/MC-R80	90.4	4.7	5
CNT/MC-R90	89.9	6.2	7
CNT/MC-D80	60.7	1.7	3
CNT/MC-D90	58.1	9.0	16

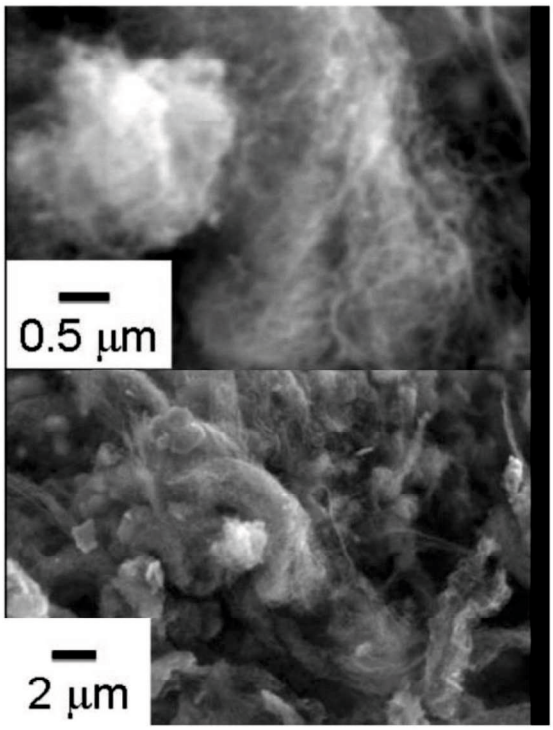

Fig. 2.5 SEM images of the CNT/MC-D90 composite.

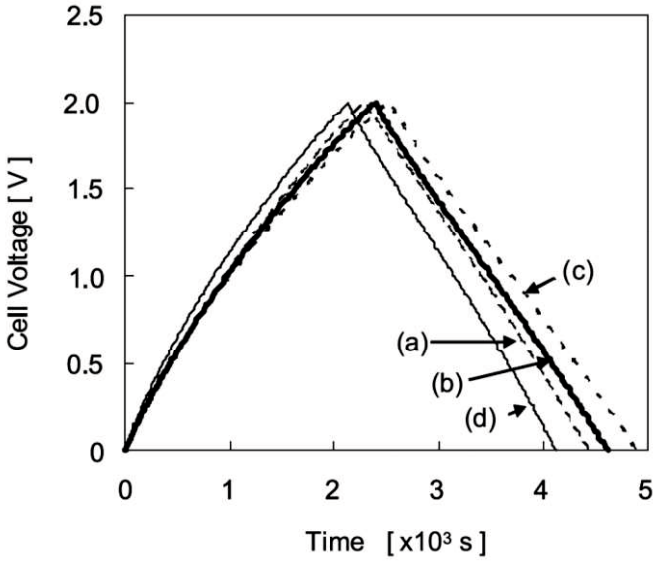

Fig. 2.6 Constant current charge-discharge profiles of the symmetric capacitor cells. Electrode: (a) CNT, (b) VGCF/MC-D90, (c) VGCF/MCR90, (d) VGCF/MC-R80. Electrode mass: (a) 25.4 mg, (b) 31.6 mg, (c) 37.4 mg, (d) 48.1 mg. Current Density: 0.1 mA cm^{-2}.

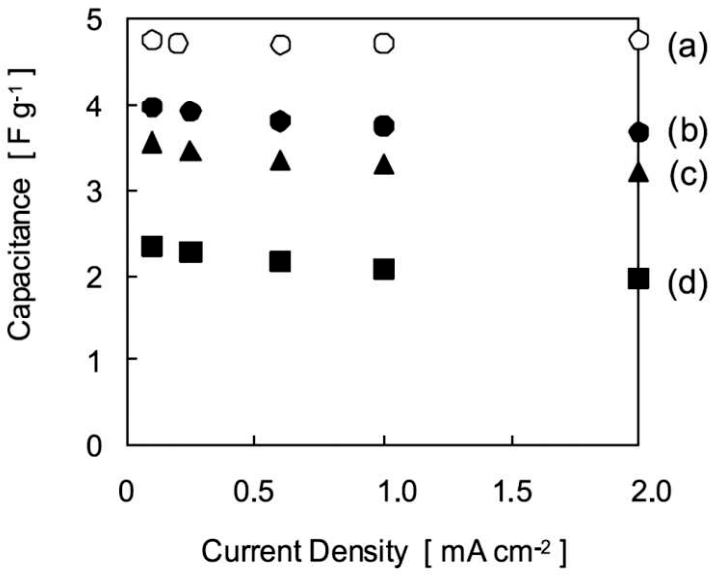

Fig. 2.7 Rate dependences of capacitances of capacitor cells with various electrodes. Electrode: (a) CNT, (b) VGCF/MC-D90, (c) VGCF/MCR90, (d) VGCF/MC-R80.

2. 4. Conclusion

The uniform mesopore created by the carbonization of R-F gel containing triblock copolymer surfactant can be reproduced on nano-carbon substrate to some extent by selecting such conditions as carbonization atmosphere, the composition (mixing ratio of the MC precursor and the substrate), and the kind of substrate. In the present trial, the composite carbons with the surface area of 100 ~ 250 m^2 g^{-1}, and the ratio of controlled mesopore volume to total pore volume reaches ca. 50 % at best. The flow condition of argon on carbonization process and the kind of substrate influences on the pore structure of the composite. The performance of test cells of double-layer capacitor including the VGCF/MC electrodes in symmetric configuration depends on the pore structure of the composite electrode, that is, the mesopore of 3.8 nm on the composite electrode provide similar double-layer capacitance of the smooth surface of the CNT electrode. In the best case of the present study the VGCF/MC composite provides rather comparable cell performance compared with the CNT cell.

2. 5. Reference

[1] E. Frackowiak and F. Béguin, *Carbon*, **39**, 937 (2000).

[2] M. Arulepp, L. Permann, J. Leis, A. Perkson, K. Rumma, A. Jänes and E. Lust, *J. Power Sources*, **133**, 320 (2004).

[3] Y. J. Kim, Y. Horie, Y. Matsuzawa, S. Ozaki, M. Endo and M. S. Dresselhaus, *Carbon*, **42**, 2423 (2004).

[4] G. J. Lee and S. I. Phun, *Electrochim. Acta*, **51**, 3029 (2006).

[5] Y. Yamada, O. Tanaike, T. -T. Liang, H. Hatori, S. Shiraishi and A. Oya, *Electrochem. Solid-State Lett*., **5**, A283 (2002).

[6] Z. Hu, M. P. Srinivasan and Y. Ni, *Carbon*, 39, 877 (2001).

[7] T. E. Rufford, D. Hulicova-Jurcakova, K. Khosla, Z. Zhu and G. Q. Lu, *J. Power Sources*, **195**, 912 (2010).

[8] M. Morita, S. Watanabe, M. Ishikawa, H. Tamai and H. Yasuda, *Electrochemistry*, **69**, 462 (2001).

[9] M. Egashira, S. Okada, Y. Korai, J. Yamaki and I. Mochida, *J. Power Sources*, **148**, 116 (2005).

[10] T. Kyotani, T. Nagai, S. Inoue and A. Tomita, *Chem. Mater*, **9**, 609 (1997).

[11] S. Yoon, J. Lee, T. Hyeon and S. M. Oh, *J. Electrochem. Soc.*, **147**, 2507 (2000).

[12] H. Zhou, S. Zhu, M. Hibino and I. Honma, *J. Power Sources*, **122**, 219 (2003).

[13] C. Vix-Guterl, S. Saadallah, K. Jurewicz, E. Frackowiak, M. Reda, J. Parmentier, J. Patarin and F. Béguin, *Mat. Sci. Eng. B*, **108**, 148 (2004).

[14] A. B. Fuertes, F. Pico and J. M. Rojo, *J. Power Sources*, **133**, 329 (2004).

[15] A. B. Fuertes, G. Lota, T. A. Centeno and E. Krackwiak, *Electrochim. Acta*, **50**, 2799 (2005).

[16] W. Xing, S. Z. Qiao, R. G. Ding, F. Li, G. Q. Lu, Z. F. Yan and H. M. Cheng, *Carbon*, **44**, 216 (2006).

[17] M. Sevilla, S. Álvarez, T. A. Centeno, A. B. Fuertes and F. Stoeckli, *Electrochim. Acta*, **52**, 3207 (2007).

[18] S. Tanaka, N. Kishiyama, Y. Egashira and K. Ueyama, *Chem. Commun*., **16**, 2125 (2005).

[19] S. Tanaka, A. Doi, N. Nakatani, Y. Katayama and Y. Miyake, *Carbon*, **47**, 2688 (2009).

[20] C. Niu, E. K. Sichel, R. Hoch, D. Moy and H. Tennent, *Appl. Phys. Lett.*, **70**, 1480 (1997).

[21] K. H. An, W. S. Kim, Y. S. Park, Y. C. Choi, S. M. Lee, D. C. Dhung, D. J. Bae, S. C. Lim and Y. H. Lee, *Adv. Mater.*, **13**, 497 (2001).

[22] B. Zhang, J. Liang, C. L. Xu, B. Q. Wei, D. B. Ruan and D. H. Wu, *Mat. Lett.*, **51**, 539 (2001).

[23] J. H. Chen, W. Z. Li, D. Z. Wang, S. X. Yang, J. G. Wen and Z. F. Ren, *Carbon*, **40**, 1193 (2002).

[24] Q. L. Chen, K. H. Xue, W. Shen, F. F. Tao, S. Y. Yin and W. Xu, *Electrochim. Acta*, **49**, 4157 (2004).

[25] Y. Honda, T. Ono, M. Takeshige, N. Morihara, H. Shiozaki, T. Kitamura, K. Yoshikawa, M. Morita, M. Yamagata and M. Ishikawa, *Electrochem. Solid-State Lett.*, **12**, A45 (2009).

Chapter 3.

The Influence of Graphitic Structure of Carbon Electrode on Aging Behavior of Electric Double Layer Capacitor

Abstract

The double-layer capacitors and their degradation after aging process for nano-fibrous carbon electrodes with various graphitic structures have been compared. The nano-fibrous carbon with amorphous structure has successfully been prepared from biomass precursor. The nano-fibrous carbons with graphitic and amorphous structures exhibit similar specific surface area and double-layer capacitance. However, the change of the capacitances of the cells consisting of both carbons by the aging process under high temperature and high voltage condition are different. The amorphous nano-fibrous carbon electrode provides capacitance decrease by the deposit on electrode, while the graphitic nano-fiber provides capacitance increased likely due to the gas evolution.

3. 1. Introduction

Electric double layer capacitors (EDLCs) are rechargeable electrical energy storage devices based on the capacitance of electric double layer without charge transfer reaction. Therefore, EDLCs have been expected to have long cycle life compared with batteries [1-3]. However, practical EDLCs frequently show severe capacitance degradation at shorter time than expected. Many attempts have been made to understand the degradation mechanism for EDLCs. Such parasitic reactions as the decomposition of electrolyte or deformation of electrode have been proposed as the cause of the degradation. The existences of moisture impurity in non-aqueous or surface oxygen-containing functional groups can also promote the decomposition of electrolyte [4-10].

For most carbonaceous materials, surface functional groups exist on the edge of graphitic planes. Therefore, the graphitic structure of carbon electrode is expected to give significant influence on the aging behavior for EDLCs. However, the detail of such influence is still unclear. The difficulty of revealing the degradation mechanism is arisen by the closed pore structure of activate carbon (AC) electrodes used in conventional EDLCs devices [11-13]. In the present study, fibrous nano-carbons having an exposed outer surface were applied in order to elucidate the effects of graphitic structure of carbon surface. Vapor-grown carbon fiber (VGCF) has been well known as fibrous nano-carbon with exposed graphene surface. Here alternative fibrous nano-carbon with amorphous carbon structure has been prepared by the carbonization of cellulose fiber derived from biomass, and its electrochemical behavior, in particular concerning on aging, is compared with VGCF.

3. 2. Experimental

3. 2. 1. Preparation of fibrous nano-carbon derived from biomass

An edible gel consisting of nano-fibrous cellulose named as 'Nata-de-Coco' has used as a carbon precursor [14]. The 'Nata-de-Coco' gel was milled and dispersed in de-ionized water, with ultrasonic treatment for the removal of impurity contained. Then, the suspension was filtrated, washed with de-ionized water several times, and dried to remove entrapped water. The obtained cellulose nano-fiber was carbonized at 1273 K under the argon flow, with heating rate of 10 $Kmin^{-1}$. The content of impurity in the product was confirmed by X-ray diffraction (XRD; Ultima IV Protectus, RIGAKU, Japan) and the elemental analyses. The obtained biomass-derived carbon nano-fiber, here-after denoted as BCNF, was characterized by transmitted electron microscope (TEM; JEM-6320F, JEOL, Japan). Surface area and pore structure of BCNF was estimated from nitrogen adsorption (NOVA2000, Quantachrome) isotherm. VGCF was purchased from Showa Denko Co.

3. 2. 2. Electrochemical studies of fibrous nano-carbon electrodes

Powder of BCNF or VGCF was molded with 10 wt% of poly(tetrafluoroethylene) (PTFE; Mitsui Fluorotech Co., Japan) binder, cut into disk shape with 7 or 12 mm in diameter and 0.30 mm of thickness. The masses of BCNF electrodes are approximately 7.0 or 24 mg, and those of VGCF are 4.0 or 13 mg, respectively. PTFE-lined sealed cells, 3-electrode configuration with a carbon/PTFE disk as working electrode, a platinum plate as counter electrode, and silver wire as quasi-reference electrode for cyclic voltammetry (CV) and 2-electrode configuration with two carbon/PTFE disks with similar diameter placed at both side of glass filter separation for the constant-current tests, were assembled, respectively. The solution, 1 mol dm^{-3} tetraethyl ammonium tetrafluoroborate ($TEABF_4$; Kishida Chemicals Co., Japan) dissolved into propylene carbonate (PC; Kishida Chemicals Co., Japan) was used as electrolyte. Each cell was assembled in a glove box filled with argon, and placed in a sealed vessel for measurements outside of the glove box. Cyclic voltammetry was measured by using a potentiostat (Versastat4, Princeton Applied

Research Inc.) between -1.0 and 1.0 V at the scan rate of 50 mV s^{-1}. The constant current charge-discharge experimental was conducted under such conditions the cut-off voltage of 0 to 2 V, and the prescribed current, using a cycler (BTS- 2004 Nagano Co., Japan).

The aging behavior of each electrode was monitored by the following sequence; the constant-voltage storage was conducted at 3.5 V for 100 h under the constant temperature of 333 K controlled by a temperature chamber (SU-241, Espec Co., Japan). The cell capacitances were estimated from the discharge profiles on the constant current charge-discharge test was conducted at 0.1 mA per square geometric area of electrode under the cut-off voltage of 0 to 2 V on 2-electrode cell at room temperature, using a cycler (BTS-2004 Nagano Co., Japan). The cell resistance of the BCNF and VGCF cells electrode after these discharging processes was confirmed by AC impedance measurements using the same apparatus as frequency response analyzer. The frequency region and AC amplitude applied in these measurements were from 10^{6} to 10^{-2} Hz, and 10 mV from OCV. The morphology of each carbon electrode after aging was observed by using scanning electron microscope (SEM; VE-8800, Keyence Co., Japan).

3. 3. Results and discussion

3. 3. 1. The structure of BCNF

The TEM image of BCNF and VGCF are shown in Fig. 3.1. Both carbons have similar fibrous feature with tens of nanometer in diameter. VGCF shows the microstructure with graphitic planes along fiber direction. In contrast, BCNF shows confirmed amorphous micro-texture. From elemental analysis, BCNF consists of 90 wt% carbon, 2 wt% hydrogen, and 7 wt% oxygen, while VGCF consists of 99 wt% carbon. The ash contents in BCNF are less than 1 wt%. The oxygen content on BCNF suggests the existence of many functional groups on its surface. The surface areas of VGCF and BCNF calculated from nitrogen adsorption isotherm are 20 and 28 $m^2 g^{-1}$, respectively. In addition, the pore size distributions of both fibrous nano-carbons show no characteristic peaks, indicating smooth surface structures of these fibrous nano-carbons.

3. 3. 2. Electrode properties of fibrous nano-carbon

The cyclic voltammograms of VGCF and BCNF under the scan rate of 50 mV s^{-1} are shown in Fig. 3.2. Both carbon electrodes exhibit typical rectangular voltammograms of double-layer capacitor electrode without redox current. The specific capacitance values calculated from the voltammograms are 1.2 and 0.8 F g^{-1} for BCNF and VGCF, respectively. The specific capacitance values divided by their specific surface area for BCNF and VGCF are 4.3 and 4.0 F cm^{-2}, respectively. The capacitance per unit surface area of BCNF is similar to that of VGCF, regardless of the graphitic structure.

3. 3. 3. Aging behavior of each carbon electrode

The charge-discharge profiles under constant-current 0.1 mA cm^{-2} before and after aging experience are shown in Figs. 3.3 (a) and 3.3 (b) for the BCNF and the VGCF cells, respectively. Both fresh cells exhibit typical EDLC charge-discharge profiles with good efficiency. The difference of capacitance for both fresh cells is caused by the difference in the mass of electrode. After the aging process, the charging profiles of both cells show

plateau above 1.75 V. The capacitance of BCNF decreases significantly by aging. In contrast, the capacitance of VGCF increases. The capacitance values of the BCNF and the VGCF cells are 0.23 and 0.15 F g^{-1}, and those of after aging are 0.18 and 0.25 F g^{-1}, respectively. The potential changes of positive and negative electrode on 2-electrode cell for BCNF and VGCF are estimated by applying silver reference electrode.

The potential profiles are shown in Figs. 3.4 (a) and 3.4 (b) for the BCNF and VGCF cells, respectively. The capacitances appear to be limited by the negative electrode for the cells regardless of aging. In addition, negative electrode of the BCNF cell on fresh cell, a plateau potential change is observed likely due to the side reaction. After aging, a plateau is observed at the profiles of both positive and negative electrodes for the BCNF cell, while in case of VGCF it appears only negative side. The Nyquist plots of fresh cells and after aging are shown in Figs. 3.5 (a) and 3.5 (b) for the BCNF and VGCF cells, respectively. The Nyquist plots of BCNF show only 45° slope, indicating diffusion limited process, and vertical rise, indicating ideal capacitor behavior, without semicircle. After aging, 45° slope regions become extended with increase of Z' intercept of high frequency region, indicating series resistance component. In constant, those of VGCF show a vertical rise with the small semicircle and on fresh cells, and show increase of the semicircle resistance after aging. The morphologies of electrodes after aging observed by SEM are shown in Fig. 3.6. The negative electrode of the BCNF cell in Fig. 3.6 (b) shows some coverage with deposits. In contrast, the positive and negative electrodes of the VGCF cell rather show fibrous textures, similar to the fresh situation. The change TEM images of VGCF before and after aging are indicated in Fig. 3.7. The electrode after aging shown in Fig. 3.7 (b) has somewhat amorphous surface, while the fresh VGCF shows graphitic surface structure. Such the change of surface graphitic structure is related to the increase of specific capacitance. From SEM and TEM observation, the products on aging process are different between BCNF and VGCF. Therefore, the capacitance degradation of BCNF is due to the decrease of the effective surface area of carbon electrode, while, etching of graphene edges by evolved gas may increase the surface area of VGCF and then increase its capacitance. The difference of aging behavior is conjectured due to the difference of structure between the carbon electrodes. However, presently it is still unclear which factors dominantly contribute the reaction. Based on these results, as electrode

materials for EDLC with high durability, the carbon materials with rich graphitic basal plane on its surface are advantageous compared with amorphous carbons.

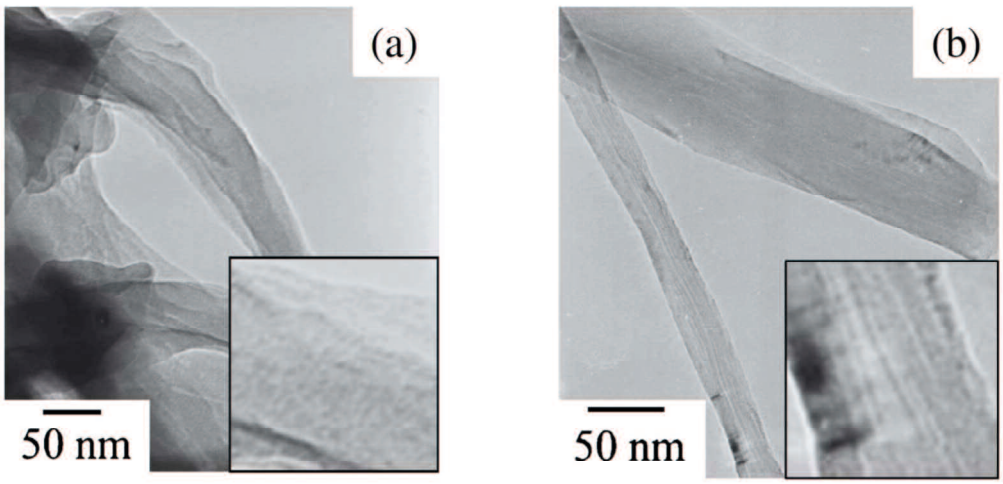

Fig. 3.1 TEM images of nano-fibrous carbons. (a) BCNF, (b)VGCF.

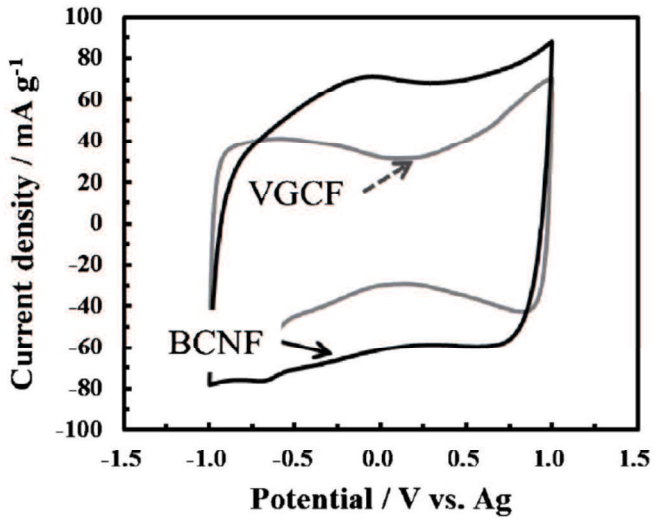

Fig. 3.2 Cyclic voltammograms of nano-fibrous carbon electrodes.
Scan rate: 50 mV s^{-1}.

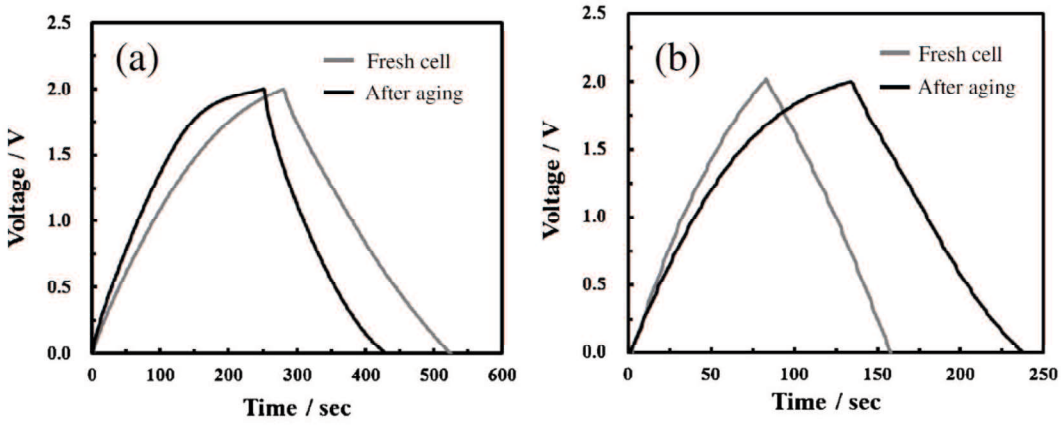

Fig. 3.3 Charge-discharge profiles of the EDLC cells consisting of nano-fibrous carbon electrodes. Current density: 0.1 mA cm^{-2}.

(a) BCNF cell, (b) VGCF cell.

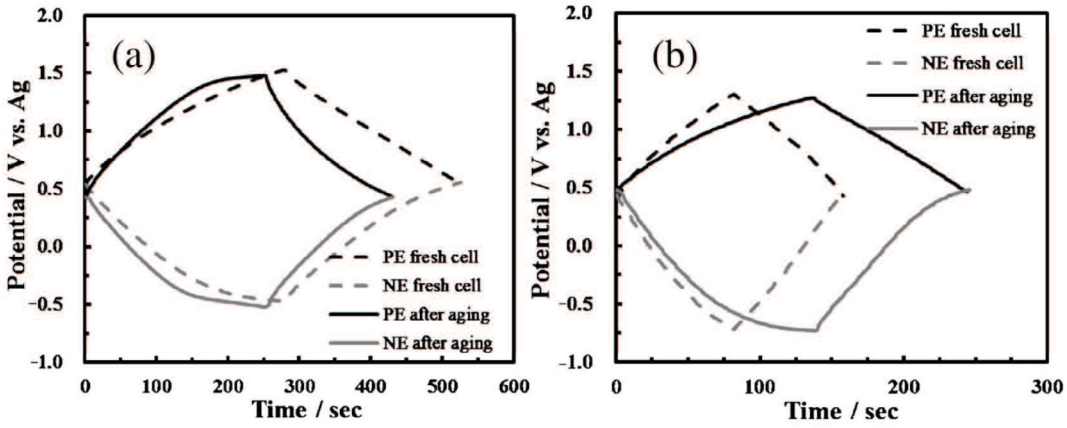

Fig. 3.4 Charge-discharge profiles for the EDLC cells consisting of nano-fibrous carbon electrodes. Current density: 0.1 mA cm^{-2}.

(a) BCNF cell, (b) VGCF cell.

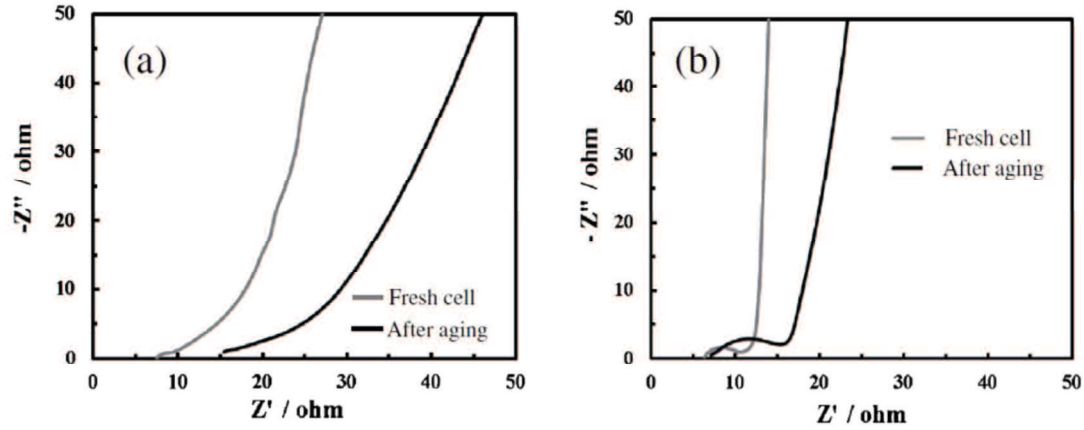

Fig. 3.5 Nyquist plots for fresh EDLC cells and the cells after aging in the immersions voltage. (a) BCNF cell, (b) VGCF cell.

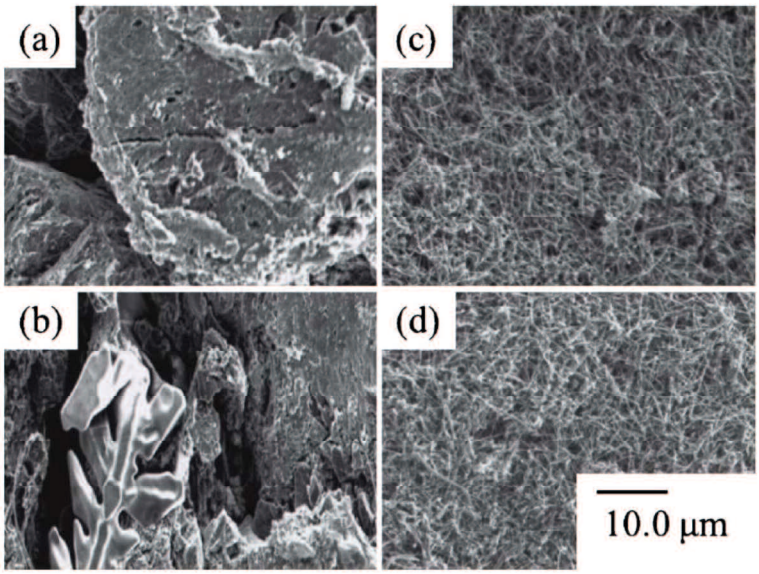

Fig. 3.6 SEM images of the electrodes after the aging test.

(a) BCNF positive electrode, (b) BCNF negative electrode, (c) VGCF positive electrode, (d) VGCF negative electrode.

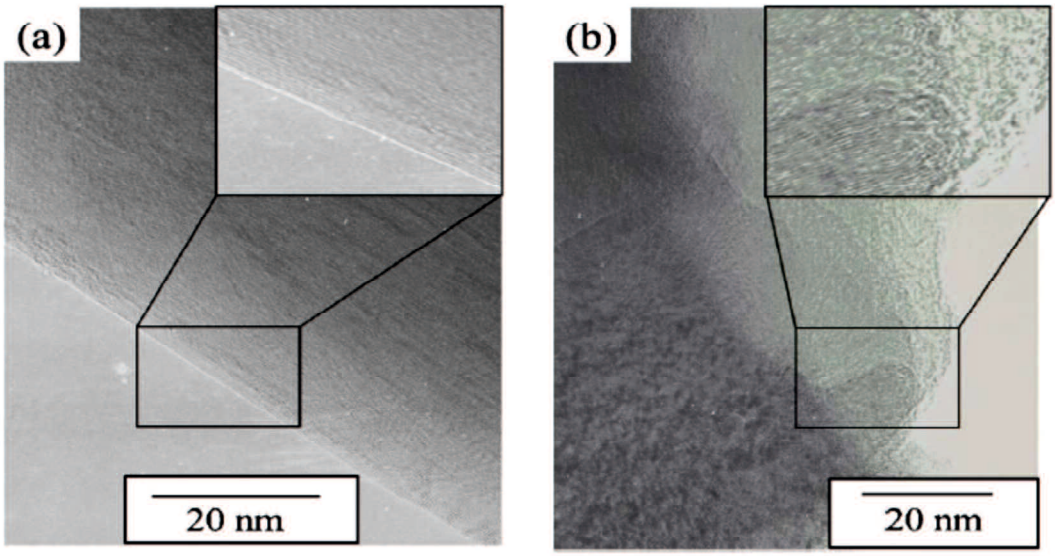

Fig. 3.7 (Color online) TEM images of fresh VGCF and the positive electrode after aging. (a) Fresh VGCF, (b) After aging.

3. 4. Conclusion

Amorphous fibrous nano-carbon, BCNF was prepared from biomass cellulose. BCNF has specific surface area of 28 $m^2 g^{-1}$, and oxygen-containing functional groups. The influence of graphitic structure of carbon electrode on the aging process can be elucidated by comparing the aging behavior the cell consisting of between BCNF and VGCF. Amorphous BCNF provides similar capacitance per unit surface area to VGCF, regardless of the different graphitic structure. On accelerating aging test by the constant voltage of 3.5 V and high temperature, BCNF provides the degradation of cell capacitance because of decreasing effective surface area of carbon electrode by deposit. In contrast, VGCF provides the increase of capacitance by surface etching.

3. 5. Reference

[1] A. D. Roberts, *J. Colloid Interface Sci.*, **41**, 23 (1972).

[2] M. Hahn, O. Barbieri, R. Gallay, and R. Kötz, *Carbon*, **44**, 2523 (2006).

[3] O. Barbieri, M. Hahn, A. Herzog, and R. Kötz, *Carbon*, **43**, 1303 (2005).

[4] O. Bohlen, J. Kowal, and D. U. Sauer, *J. Power Sources*, **172**, 468 (2007).

[5] P. Kurzweil and M. Chwistek, *J. Power Sources*, **176**, 555 (2008).

[6] R. Kötz, P. W. Ruch, and D. Cericola, *J. Power Sources*, **195**, 923 (2010).

[7] P. W. Ruch, D. Cericola, A. Foelske, R. Kötz, and A. Wokaun, *Electrochim. Acta*, **55**, 2352 (2010).

[8] O. Bohlen, J. Kowal, and D. U. Sauer, *J. Power Sources*, **172**, 468 (2007).

[9] O. Bohlen, J. Kowal, and D. U. Sauer, *J. Power Sources*, **173**, 626 (2007).

[10] H. Gualous, R. Gallay, G. Alcicek, B. Tala-Ighil, A. Oukaour, B. Boudart, and Ph. Makany, *Microelectron. Reliab.*, **50**, 1783 (2010).

[11] E. Frackowiak and F. Beguin, *Carbon*, **39**, 937 (2001).

[12] L. Wang, M. Fujita, and M. Inagaki, *Electrochim. Acta*, **51**, 4096 (2006).

[13] H. Wang, J. Varghese, and L. Pilon, *Electrochim. Acta*, **56**, 6189 (2011).

[14] M. Iguchi, S. Yamanaka, and A. Budhiono, *J. Mater. Sci.*, **35**, 261 (2000).

Chapter 4.

Properties of an Electrochemical Capacitor Based on Carbon Electrodes Derived from α-cyclodextrin

Abstract

Capacitor performances and degradation behavior of porous carbon electrodes derived from α-cyclodextrin precursor have been investigated. Porous carbons with different pore size distribution have successfully been prepared from α-cyclodextrin by changing the heating rate of carbonization. The carbonaceous materials obtained by the heating rates of 10 and 50Kmin^{-1} exhibited similar crystalline structures and elemental compositions. However, the cells with different electrodes showed different capacitance degradation modes under high temperature and high voltage conditions. The α-cyclodextrin-derived carbon having a higher ratio of mesopore volume lost its capacitance significantly at initial cycles by the passivation of electrode.

4. 1. Introduction

Electric double layer capacitors (EDLCs) are rechargeable energy storage devices based on the capacitance of electric double layer at electrode/electrolyte interface without charge transfer reaction. Porous carbon electrodes such as activated carbons (ACs) have been utilized for EDLC devices [1, 2]. Many kinds of porous carbons derived from various precursors [3, 4], with different activation processes utilizing oxidizing agents in solid, liquid and gas phases [5, 6], have so far been proposed. Recently, some porous carbons with ordered micro-structures have been prepared by so-called soft- and hard-template methods and their capacitor performances examined [7]. The EDLC performances are generally dependent on the characteristics of the porous carbon electrodes, in particular crystalline structure, pore structure and surface functional groups [8-10].

Besides the charge-discharge performances, long-term stability should be taken into consideration for designing EDLC electrodes. While EDLC is, in principle, expected to have much longer cycle life than that of a conventional battery, due to its charge storage mechanism, practical EDLC devices show severe capacitance degradation at shorter time than expected. Thus, many attempts have been made to understand the degradation mechanism of EDLCs. Parasitic reactions such as decomposition of electrolyte and/or deformation of electrode have been proposed as the main cause of the degradation [11-15]. However, details in the influences of pore structure on such parasitic reactions remain still unclear.

More recently, nano-structured carbon materials including carbon nano-rods with high specific surface area (~ 800 m^2 g^{-1}) have been prepared by simple carbonization of α-cyclodextrin acquirable from biomass with varying the heating rate [16]. These carbons are expected as alternative porous carbons because of low-cost production processes (without additional activation processes) and interesting nano-structures with uniform pore-size distribution. In the present study, the reproducibility of porous carbons with various nanostructures from α-cyclodextrin has been assessed under different heating rates, and their electrode properties have been compared with each other. Especially, influences of the porous structure on the aging behavior of EDLCs have been focused as

well as on the capacitance and rate capability.

4. 2. Experimental

4. 2. 1. Preparation of porous carbons having different pore structures

Porous carbons were prepared by the carbonization of α-cyclodextrin (Kanto Chemical) precursor up to 1273 K with different heating rates of 10 and 50 K min^{-1}, followed by continuous heating at 1273 K for 20 h. The products obtained by the former and the latter heating rates are denoted as CyDC10 and CyDC50, respectively. The microscopic structures of the obtained carbons were observed by a transmission electron microscope (TEM; JEM-6320F, JEOL, Japan), and their crystalline structures were confirmed by X-ray diffraction (XRD; Ultima IV Protectus, Rigaku, Japan). The contents of surface functional groups were estimated by elemental analysis. Specific surface area and pore-size distribution of CyDCs were respectively estimated by BET analyses and BJH method from nitrogen adsorption isotherms (NOVA2000, Quantachrome).

4. 2. 2. Electrochemical properties of CyDCs

CyDC powder was molded with 10 wt% of poly(tetrafluoroethylene) (PTFE; Mitsui Fluorochemical, Japan) binder, and the resulting sheet was cut into a disk with 7 or 12 mm in diameter. The thickness of the electrode disk was set to 0.30 mm and the loading mass was about 18 mg cm^{-2} for CyDC10 and about 20 mg cm^{-2} for CyDC50. A PTFE cell with 3-electrode configuration consisting of a carbon/PTFE disk as the working, a platinum plate as the counter and silver wire as the quasi-reference electrode was used for cyclic voltammetry (CV). For constant-current charge-discharge tests, 2-electrode configuration with two parallel carbon/PTFE disks and a glass-filter separator was utilized. The accelerated aging tests and AC impedance measurements were also conducted using the 2-electrode cell. The solution of 1 mol dm^{-3} tetraethylammonium tetrafluoroborate ($TEABF_4$; Kishida Chemicals, Japan) in propylene carbonate (PC; Kishida Chemicals, Japan) was used as the electrolyte. Each cell was assembled in a glove box filled with dry argon, and placed in a sealed vessel for the measurements outside of the glove box. The electrochemical measurements including the rate capability estimation of the EDLC cell were conducted using a potentiostat (Versastat4, Prinston Applied

Research) with a potential range between -1.0 and 1.0 V at prescribed scan rates. The constant-current charge-discharge experiments were carried out under such conditions as the cut-off voltage of 0 to 2 V, at the prescribed current density, using a charge-discharge cycler (BTS-2004 Nagano, Japan). The accelerated aging behavior of each electrode was monitored by the following procedure. Constant cell voltage of 3.5 V was applied for 5 h under constant temperature of 333K (60 ^{o}C), controlled by a constant-temperature chamber (SU-241, Espec, Japan), and then discharged under constant-current of 1.0 mA per unit geometric area of the electrode to 0 V. This procedure was repeated for 20 cycles by using the same cell cycler as described above. The cell resistance after this accelerated aging process was estimated by AC impedance methods using a frequency response analyzer (Versastat4) with a frequency range from 10^{6} to 10^{-2} Hz.

4. 3. Results and discussion

4. 3. 1. Characterization of CyDCs

Typical TEM images of CyDCs are shown in Fig. 4.1, where dotted white lines are added as the outlines of the particles for visualization. It is not so clear but we found that CyDC10 has larger particle size (< 200 nm) than CyDC50 (< 50 nm). The different heating rates during the carbonization process tended to provide different particle size. From XRD pattern, both CyDCs were found to have similar amorphous structure. The specific surface area obtained from nitrogen adsorption isotherms using BET analyses was 754 m^2 g^{-1} for CyDC10 and 364 m^2 g^{-1} for CyDC50. The pore size distributions obtained by BJH method are shown in Fig. 4.2. While the surface of CyDC10 is mostly microporous, CyDC50 has different distribution of mesopore region. The results of calculation for total pore volume (V_{total}), micropore volume (V_{micro}) and mesopore/micropore volume ratio (V_{meso}/V_{micro}; $V_{meso} = V_{total} - V_{micro}$) are summarized in Table 4.1. We found a tendency that CyDC10 has different particle size, specific surface area and the ratio of mesopore volume from those of CyDC50. It is suggested that α-cyclodextrin is once melt by thermal treatment, and then formed pore structures through the gasification, where the gas generation speed is different for the different heating rates. The results of elemental analysis showed that CyDC10 contains 90 wt% of C, 1.3 wt% of H, and 7.9 wt% of O, while CyDC50 contains 95 wt% of C, 0.9 wt% of H, and 4.2 wt% of O. The amount of each element per unit surface area calculated from these data is listed in Table 4.2. This suggests that the amounts of functional groups at unit surface area are almost the same for both CyDCs. Although our present results are not consistent with those previously reported on the nano-structure of CyDC by John, et al. [16], differences in particle size and the ratio of mesopore volume between CyDC10 and CyDC50 are quite interesting, and the comparative study on capacitor performances for these carbons is worth to be examined.

4. 3. 2. Electrode properties of CyDCs

Cyclic voltammograms of CyDCs under a scan rate of 2 mV s^{-1} are shown in Fig. 4.3.

Both CyDC electrodes gave typical rectangular shapes of double-layer charging without any redox currents. The specific capacitance values calculated from the voltammograms were 40 and 19 F g^{-1} for CyDC10 and CyDC50, respectively. This trend in the specific capacitance is consistent with the specific surface area obtained by BET method. Here, the capacitance per unit real surface areas is calculated to be 5.3 mF m^{-2} for CyDC10 and 5.2 mF m^{-2} CyDC50. Both of the specific capacitance (F g^{-1}) and the capacitance per unit surface area (F m^{-2}) are much smaller than those of activated carbon electrodes used in conventional EDLCs, which is probably due to insufficient utilization of the micropores, and to insufficient wettability toward the organic electrolyte. From a practical viewpoint, the utilization of the surface area and the wettability of the electrode should be improved by an adequate 'activation' process. Fig. 4.4 shows the dependence of the specific capacitance on the scan rate in the CV experiments. Both electrodes exhibit capacitance decrease by the increase in the scan rate. However, CyDC50 shows better rate capability than CyDC10, which is probably related with higher amounts of mesopore at the surface of CyDC50.

4. 3. 3. Accelerated aging behavior of CyDCs

Variations in the cell capacitance with the cycle number during the accelerated aging test are plotted in Fig. 4.5 (a), and the normalized capacitance by the first cycle is also shown in Fig. 4.5 (b) as a function of the cycle number. The capacitance of the CyDC10 and the CyDC50 cells at the first cycle was 14 and 6 F g^{-1}, respectively. The cell capacitance decreased with the increase in the cycle number regardless of the electrode. The cell capacitance at 20th cycle was down to about 40 % of the initial cycle for CyDC10, while it decreased to about 16 % for CyDC50 [Fig. 4.5 (b)]. That is, the capacitance decrease in the CyDC50 was much severer than the CyDC10 cell. As the states of the crystalline structure and surface functional groups were almost the same for both carbons, the differences in the ratio of mesopore volume and the nano-structure would be responsible for the difference in the accelerated aging behavior. That is, CyDC50 has a larger ratio of mesopore on its surface than that of CyDC10, whose difference will influence the aging behavior significantly. Nyquist plots of AC impedance measured for

the fresh CyDC cells and for the cells after aging are shown in Figs. 4.6 (a) and 4.6 (b), respectively. The plots of the fresh cells showed semicircles at higher frequency regions, assigned to charge-transfer (interfacial) resistance, and linear parts with about 45^{o} slope in lower frequency regions which are assigned to diffusion-limited processes. After the accelerated aging, the semicircle and 45^{o} slope line regions of the cell consisting of CyDC10 become slightly extended with an increase in Z' intercept at the high frequency region, namely a series-resistance component increased. In contrast to this, the cell consisting of CyDC50 showed a two-semicircle resistance after the aging. This behavior indicates that charge-transfer resistance increased significantly with the cycle repeated. In the authors' previous work, decomposition product of the electrolyte was observed at nano-fiber electrode after the accelerated aging [17]. Thus, it is suggested that the deposition of the decomposition products would occur more significantly at CyDC50 than at CyDC10. For the porous carbon having micropores with more extents, like CyDC10, the decomposition product derived from the electrolyte will deposit mainly at the "entrance" of the pores because of the limited ion diffusion rate in the micropores, which does not accompany the blocking of the pore structure. On the other hand, for the porous carbon having larger ratio of mesopore against total surface area, like CyDC50, the deposition of the decomposition products can initially occur inside the pores because of the relatively fast mass-transport in the mesopore structures. The coverage of the pores by the decomposition product inside the pores would reduce the capacitance significantly, especially at initial cycles.

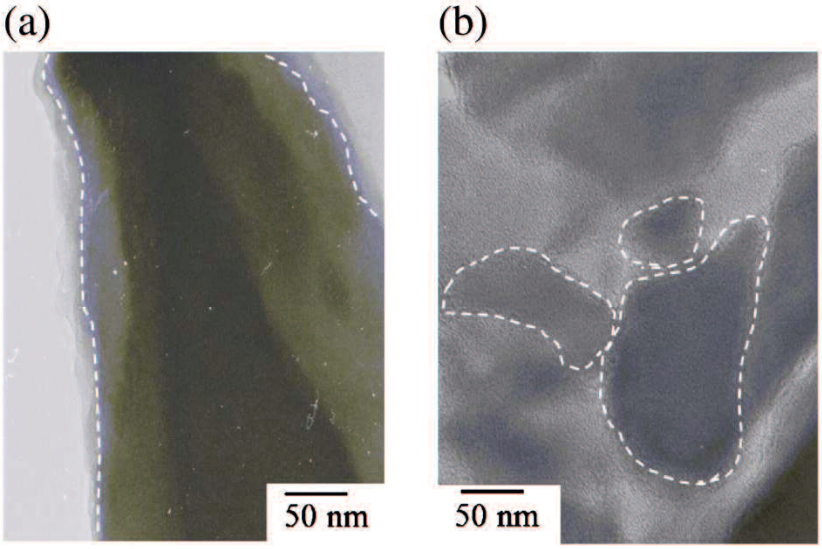

Fig. 4.1 (Color online) TEM images of CyDCs. (a) CyDC10, (b) CyDC50. Dotted white lines indicate the outlines of the particles for visualization.

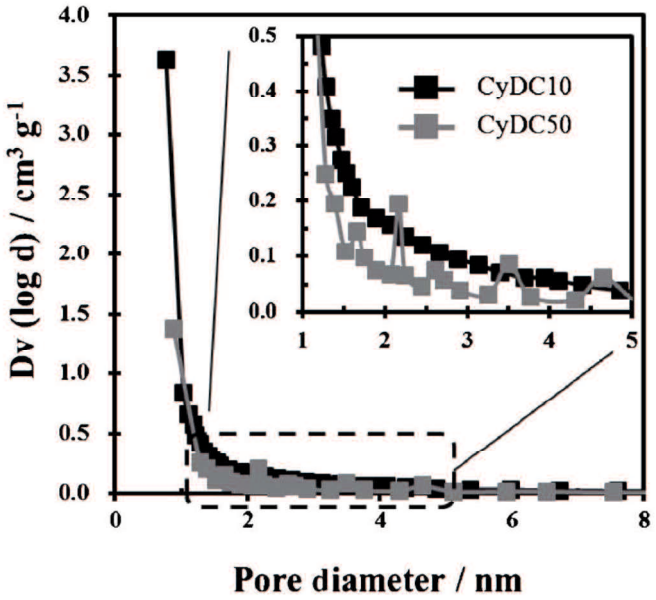

Fig. 4.2 Pore size distribution of CyDCs. CyDC10: black line, CyDC50: gray line.

Table 4.1 N_2 sorption data of CyDCs prepared from α-cyclodextrin

	SSA ($m^2\,g^{-1}$)	V_{total} ($\times10^{-2}\,cc\,g^{-1}$)	V_{micro} ($\times10^{-2}\,cc\,g^{-1}$)	V_{meso}/V_{micro}
CyDC10	754	40.0	14.7	1.7
CyDC50	364	19.5	4.7	3.2

Table 4.2 Elemental analyses of α-cyclodextrin derived carbons

	C (%)	H (%)	O (diff. %)	H/SSA ($\times10^3\,mol\,m^{-2}$)	O/SSA ($\times10^3\,mol\,m^{-2}$)
CyDC10	90	1.3	0.9	17	6.6
CyDC50	95	0.9	4.2	26	7.2

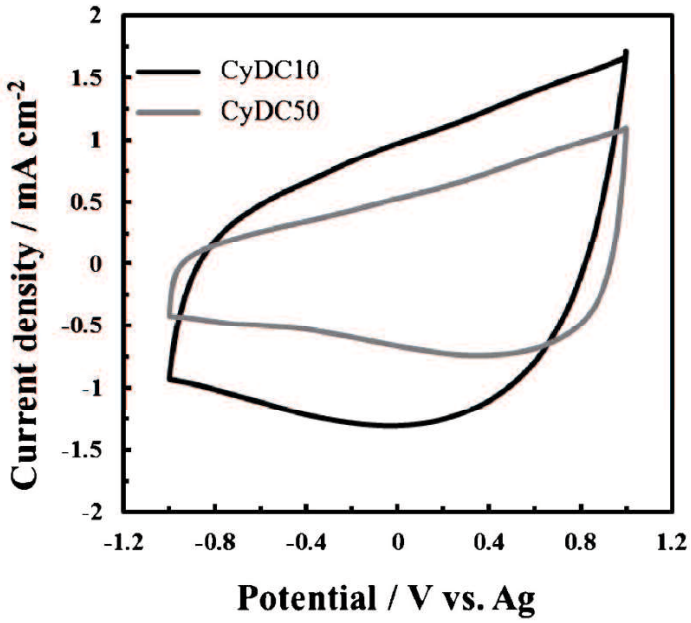

Fig. 4.3 Cyclic voltammograms of CyDCs in 1 mol dm^{-3} $TEABF_4$/PC. Scan rate: 2 mVs^{-1}.

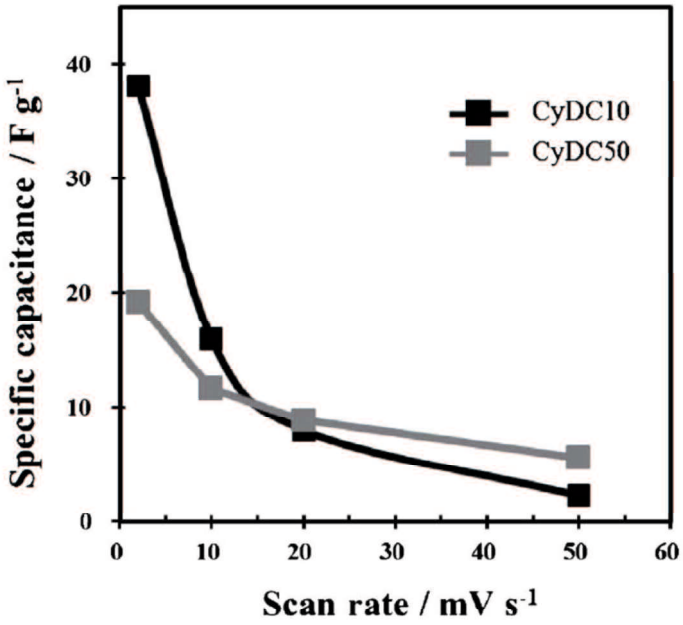

Fig. 4.4 Specific capacitance of CyDCs as a function of the scan rate. CyDC10: black line, CyDC50: gray line.

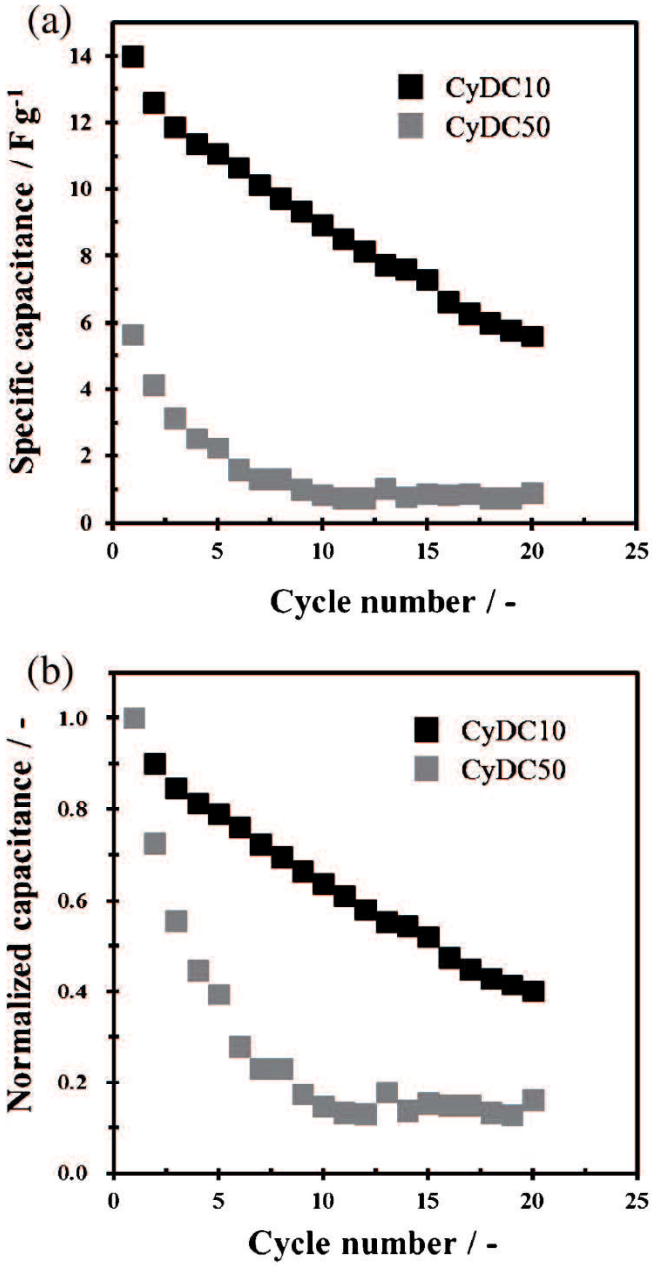

Fig. 4.5 Variations in the cell capacitance with the cycle number during the accelerated degradation test. (a) Variations in the cell capacitance, (b) Variations in the normalized capacitance with respect to the capacitance at the first cycle.

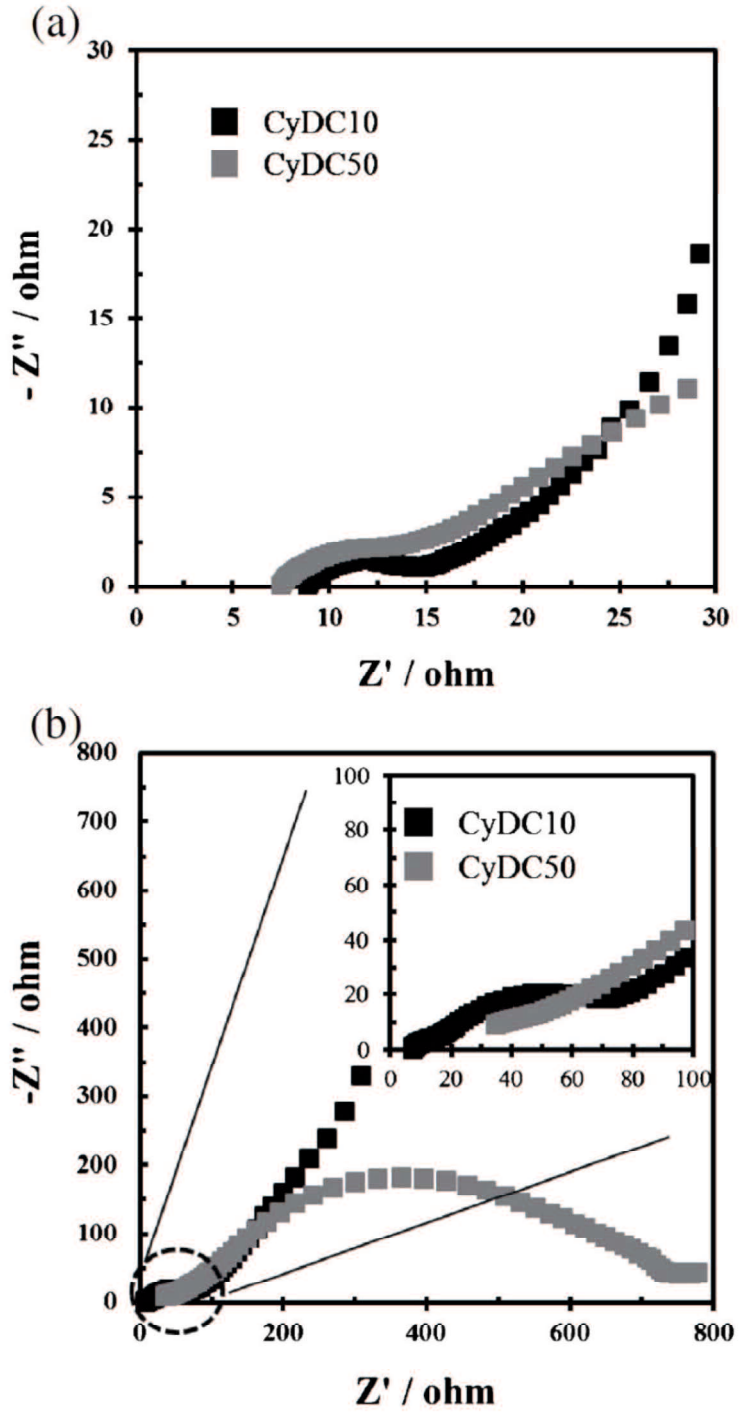

Fig. 4.6. Nyquist plots of the AC impedance measured for the CyDCs cells. (a) fresh cells, (b) after the accelerated aging.

4. 4. Conclusion

Carbons having different nano-structures were obtained by simple carbonization of α-cyclodextrin with different heating conditions: CyDC10 has larger particle size with significant micropores and CyDC50 has smaller particle size with higher ratio of mesopore volume. The rate capability of the double-layer capacitance depended on the nano-structures of the α-cyclodextrin-derived carbons (CyDCs). The accelerated aging tests using server cycling conditions (constant-voltage charging at 3.5 V for 5 h at 333 K) showed that CyDC50 having higher ratio of mesopore volume leads to the degradation of the cell capacitance significantly, compared with that of CyDC10. The AC impedance results after the accelerated aging tests suggest that the differences in the decomposition process of the electrolyte component are responsible for such degradation process.

4. 5. Reference

[1] A. Lewandowski and M. Galinski, *J. Power Sources*, **173**, 822 (2007).

[2] R. Kötz and M. Carlen, *Electrochim. Acta*, **45**, 2483 (2000).

[3] T. Morishita, Y. Soneda, T. Tsumura, and M. Inagaki, *Carbon*, **44**, 2360 (2006).

[4] W. Qiao, Y. Korai, I. Mochida, Y. Hori, and T. Maeda, *Carbon*, **40**, 351 (2002).

[5] S. H. Yoon, S. Lim, Y. Song, Y. Ota, W. Qiao, A. Tanaka, and I. Mochida, *Carbon*, **42**, 1723 (2004).

[6] M. M. Sabio, C. Almansa, and F. R. Reinoso, *Carbon*, **41**, 2113 (2003).

[7] S. Han, K. T. Lee, S. M. Oh, and T. Hyeon, *Carbon*, **41**, 1049 (2003).

[8] O. Barbieri, M. Hahn, A. Herzog, and R. Kötz, *Carbon*, **43**, 1303 (2005).

[9] D. L. Castelló, D. C. Amorósa, A. L. Solano, S. Shiraishi, H. Kurihara, and A. Oya, *Carbon*, **41**, 1765 (2003).

[10] L. Wang, M. Toyoda, and M. Inagaki, *New Carbon Materials*, **23**, 111 (2008).

[11] O. Bohlen, J. Kowal, and D. U. Sauer, *J. Power Sources*, **172**, 468 (2007).

[12] P. Kurzweil and M. Chwistek, *J. Power Sources*, **176**, 555 (2008).

[13] R. Kötz, P. W. Ruch, and D. Cericola, *J. Power Sources*, **195**, 923 (2010).

[14] P. W. Ruch, D. Cericola, A. Foelske, R. Kötz, and A. Wokaun, *Electrochim. Acta*, **55**, 2352 (2010).

[15] H. Gualous, R. Gallay, G. Alcicek, B. Tala-Ighil, A. Oukaour, B. Boudart, and Ph. Makany, *Microelectron. Reliab.*, **50**, 1783 (2010).

[16] J. E. St. Dennis, P. Venkataraman, J. He, V. T. John, S. J. Obrey, R. P. Currier, M. Lebrón-Colón, F. J. Sola, and M. A. Meador, *Carbon*, **49**, 718 (2011).

[17] M. Tokita, M. Egashira, N. Yoshimoto, and M. Morita, *Electrochemistry*, **80**, 752 (2012).

Chapter 5.

Degradation Characteristics of Electric Double-Layer Capacitors Consisting of High Surface Area Carbon Electrodes with Organic Electrolyte Solutions

Abstract

Aging behavior of electric double-layer capacitor cells consisting of high surface area carbon electrodes with organic electrolyte solutions has been examined under high voltage and high temperature cycling conditions. Influences of the electrolyte components on the performance degradation were investigated for the cells using different electrolyte compositions. The use of acetonitrile (AN) as the electrolyte solvent led to higher cycling capacitance of the cell than the cells using such alkyl carbonate solvents as propylene carbonate (PC) or ethylene carbonate mixed with dimethyl carbonate (EC+DMC, 1:1 by volume) under moderate cycling conditions. However, when the cycling was done at higher operation voltage (> 3.5 V), significant capacitance degradation was observed for the cells using AN-based electrolytes. The EDLC cells with the carbonate-based electrolytes showed moderate degradation behavior even at higher operation voltage. With respect to the electrolytic salt, cells using $LiBF_4$ generally showed lower durability than the cells using tetraethylammonium salt, $TEABF_4$, especially under high operation voltage (> 3.5 V) conditions. The mechanisms of the capacitance decreasing with the cycle repeated are discussed.

5. 1. Introduction

Electric double layer capacitors (EDLCs) have attracted much attention as efficient electrochemical power devices in which the charge storage processes proceed *via* the electrostatic force at the electrode/electrolyte interface [1-3]. Because of their simple energy storage mechanisms, EDLCs can provide higher specific power (~10 kW kg^{-1}) and longer cycle life (~100,000 cycle) than rechargeable battery systems such as lithium-ion and nickel/metal-hydride batteries, and higher specific energy (~10 Wh kg^{-1}) than such conventional capacitors as aluminum electrolytic capacitor [4, 5]. Owing to these specific advantages, EDLCs have been utilized in mobile electronics, stationary applications, and even transportation systems, eg., memory back-up use, uninterruptible power system (UPS), and hybrid electric vehicles (HEVs) [6-8]. However, specific energy (Wh kg^{-1}) and energy density (Wh m^{-3}) of EDLCs are generally much lower than those of modern battery systems like lithium-ion battery in which chemical (faradaic) processes are utilized. Therefore, many attempts have been reported on increasing the specific energy (or energy density) of the capacitor system, especially for the large-scale application area.

As the specific energy (or energy density) of EDLC, U [Wh kg^{-1}, Wh m^{-3}], is expressed by eq. (5.1),

$$U=1/2CV^2 \tag{5.1}$$

where C is the specific capacitance (or capacitance density) [F kg^{-1}, F m^{-3}] and V is the operation voltage [V], enhancing the specific capacitance and/or extending the operation voltage of the electrode materials are practically efficient to realize the capacitor devices having higher specific energy (or energy density). With respect to increasing the specific capacitance, many attempts have been published on utilizing controlled nano-structure carbon with pseudo-capacitance of metal-oxides [9, 10] or conductive polymers [11, 12]. On the other hand, extending the operation voltage of the capacitor device leads not only to higher specific energy but also to higher specific power, P [W kg^{-1}], because both of them are proportional to square of the operation voltage, as shown in eqs. (5.1) and (5.2),

$$P = V^2/Z \tag{5.2}$$

where Z denotes the impedance of the power device [Ω]. Thus, the wider operation voltage has become a main issue in developing an advanced EDLC device [13, 14]. On

this context, novel electrolyte systems possessing wider potential windows have been introduced in the capacitor device to obtain higher specific energy and power.

Typical EDLC cells are constructed by activated carbons (ACs) as main active electrode materials due to their high specific surface area (~2000 m^2 g^{-1}), and organic electrolyte solutions such as tetraethylammonium tetrafluoroborate ($TEABF_4$) or triethylmethylammonium tetrafluoroborate ($TEMABF_4$) dissolved in propylene carbonate (PC) or acetonitrile (AN) with around 1 mol dm^{-3} (M) concentration. For such an electrode/electrolyte system, durability of charge-discharge cycling becomes lowered when the cycles are done under higher voltage than *ca.* 2.7 V, especially at higher temperature than ambient one. The electrochemical decomposition of the electrolyte components tends to occur under highly polarized conditions, in which oxygen-containing surface functionalities of the carbon-based electrodes would participate in the degradation process [15]. That is, the EDLC performances would be significantly degraded under the high voltages operation.

From the above described viewpoint, the aging behavior of EDLC device under high voltage conditions has been investigated by many research groups. Structural factors of carbon electrodes, such as pore size distributions and surface functional groups, and the electrolyte components (the electrolytic salts and the solvents) affecting the degradation behavior of the capacitor device have been investigated [15-17]. We have also examined influences of the surface crystalline structures and the pore size distributions of carbon materials on the degradation behavior by using model electrodes, and then proposed different degradation mechanisms depending on the carbon structure [18, 19].

On the other hand, the organic solvents tend to contribute to the degradation reaction at the higher voltage usage of EDLC. In some cases, an undesired process accumulates a polymer-like passivation film on the electrode surface, being a possible cause of the degradation behavior of EDLC [20-22]. In the present work, we have investigated the influences of the electrolyte components on the degradation behavior of EDLC using high specific surface area carbon electrodes. The effects of the electrolyte composition on the double-layer capacitance of carbon electrodes with different pore structures have already been reported [19]. In this paper, charge-discharge cycling performances and their degradation characteristics are investigated for EDLCs with conventional AC-based

electrodes as a function of the electrolyte composition under elevated temperature conditions.

5. 2. Experimental

5. 2. 1. Preparation of AC-based electrode

Aging behavior of EDLC cell was monitored by using symmetric AC-based electrode combinations with organic electrolyte solutions containing different components. The sheet electrode was composed of 85 mass% AC (YP-50F, Kuraray Chemical) as the active material, 5 mass% acetylene black (AB, Denki Kagaku Kogyo) as a conducting support and 10 mass% poly(tetrafluoroethylene) (PTFE, Du Pont-Mitsui Fluorochemicals) as a binder. It was cut into a disc of 10 mm diameter and 200 μm thickness, whose average mass was 6.5±0.5 mg. The AC sheet electrode was pressed onto an Al mesh current-collector. The resulting disc electrode was dried sufficiently under a vacuum at 120 °C for 20 h or longer before use.

5. 2. 2. Characterization of aging behavior

A coin-type cell (2032, Mic-Lab) was constructed with a glass filter separator between two symmetric positive and negative AC-based electrodes. Acetonitrile (AN), propylene carbonate (PC), or a 1:1 mixture (by volume) of ethylene carbonate and dimethyl carbonate (EC+DMC) was used as the organic solvent of the electrolyte solution. All the solvents were obtained from Kishida Chemicals (Battery Grade) and used as received without further purification. The electrolytic salt was tetrafluoroborate salt of lithium ($LiBF_4$, Kishida Chemicals) or tetraethylammonium ($TEABF_4$, Kishida Chemicals) which was dissolved in each organic solvent to make commonly 1mol dm^{-3} (M) of the concentration. The preparation of the electrolytic solutions and construction of the coin cells were conducted in a glove box (Miwa Seisakusho) filled with high-purity dry Ar. It was confirmed that the contents of the residual water in the resulting electrolytic solutions were less than 50 ppm.

The aging behavior was monitored during the charge-discharge cycling under accelerated conditions. Constant current of 2.0 mA cm^{-2} (per geometric area: corresponding to *ca.* 0.3 A g-$carbon^{-1}$) was applied for both charging and discharging at 333K (60 ^{o}C), using a battery cycler (BTS-2004, Nagano). The upper voltage limit for

charging was varied from 3.0 to 4.0 V, while the lower voltage limit for discharging was kept to 0 V throughout the experiments.

The surface of the AC electrode was observed by a scanning electron microscope (SEM, JSM-7600; JEOL Ltd.) before and after the aging test. The aged electrode was rinsed thoroughly with DMC solvent and dried in an inactive atmosphere under a mild condition before SEM observation.

In order to investigate the degradation process at each electrode (positive or negative), we utilized a cell re-assembling technique. After the continuous cycling, the aged cell was carefully disassembled in the glove box, and then each electrode was rinsed with DMC solvent to remove surface contaminants. After drying the aged electrode, a new coin-cell was re-assembled using the aged electrode with a flesh AC-based counter electrode, together with the flesh electrolyte solution. Then, charge-discharge cycling was conducted under different constant currents (0.1 - 4.0 mA cm^{-2}) for the voltage range of 0 - 2.0 V at room temperature (*ca.* 298 K).

5. 3. Results and Discussion

5. 3. 1. Influences of the electrolyte solvent

Changes in the specific capacitance with repeated charge-discharge cycling was used as a primary criterion of the degradation of EDLC test cells constructed with different electrolyte components. Another index for the durability of the electrode was differences in the EDLC performances (specific capacitance and rate capability) of the cell that is re-assembled with the aged electrode coupled with a fresh AC counter electrode and a fresh electrolyte.

The aging characteristics of the EDLC cells using different organic solvents, AN, PC, and EC+DMC, are examined in terms of the changes in the specific capacitance with repeated charge-discharge cycling under an accelerated high voltage/high temperature condition. The voltage profiles at the 1st cycle under a constant current (2.0 mA cm^{-2}) are shown in Fig. 5.1, where the operation temperature was 333 K and the voltage limit of charging was varied from 3.0 to 3.5 V. Changes in the voltage slope have become clearer for the charging to higher voltage limit (3.5 V) for the cell using AN solvent than in the cell using carbonate solvents. On the other hand, the voltage profile during the discharge branch was rather smooth change even in the AN-based electrolyte. These results suggest that some irreversible faradaic processes would occur at the voltage region above 3 V.
The specific capacitance, C [F g^{-1}], of each cell was calculated from the slope of the discharge branch of the voltage profile, by using Eq. (5.3)

$$C = I \times \Delta t / \Delta V \times 2m \qquad (5.3)$$

where I [A] is the discharge current (typically, 1.57×10^{-3} A), Δt [s] the time required for discharging from 1 V to 0 V, ΔV [V] the change in the cell voltage (here, 1 V), in which the *IR*-drop is eliminated, and m [g] the mass of the activated material (YP-50F) at one electrode. Changes in the specific capacitance of the cells using 1 mol dm^{-3} $TEABF_4$ dissolved in AN, PC and EC+DMC are shown in Fig. 5.2 as a function of the cycle number. In the AN-based electrolyte solution, the capacitance tends to increase with the voltage limit up to 3.5 V. This phenomenon is probably caused by a kind of “electrochemical activation”. That is, the number of active sites at the carbon material can increase with the application of higher voltage, that would include an etching effect by small molecule

of AN inside the pore structure [23, 24]. On the other hand, specific capacitance of the cells using PC or EC+DMC solvent decreased gradually with the repeated cycle. This trend suggests that some side reactions form insoluble deposits on the electrode surface [18].

After the cycling tests, the test electrodes were taken from the disassembled cell and rinsed with DMC in an inert atmosphere to remove precipitates from the electrolyte salts. The surface of the resulting aged electrode was observed by SEM. Typical results of the SEM observation are presented in Fig. 5.3. Polymeric products are observed on the crack of the electrode surface that was cycled in the AN-based electrolyte (Figs. 5.3a, 5.3b), especially at the positive electrode surface (Fig. 5.3a). On the other hand, much smaller amounts of deposits are detected on the surface of the electrode that cycled in carbonate-based electrolytes, despite of some cracks (Figs. 5.3c and 5.3e).

Beside the SEM observation done for the aged electrode surface, another cell was re-constructed with coupling the aged electrode, freshly prepared counter electrode and the fresh electrolyte solution. The reconstructed cell was provided to examine the constant-current cycling at 298 K (25 °C). Fig. 5.4 shows the specific capacitance as a function of the cycling current. The cell using the aged positive electrode that cycled in AN-based electrolyte over 3.5 V charging showed significantly lower capacitance than that obtained for the cell using fresh electrodes (Fig. 5.4a). According to the SEM images of the electrode surface (Figs. 5.3a, 5.3b), deposits on the positive electrode surface is considered to be a major reason for the capacitance decrease. On the other hand, the cells reconstructed with the aged electrodes in PC- and EC+DMC-based electrolytes kept similar capacitance values even if the cycling was done at higher operation voltages (Figs. 5.4b, 5.4c). However, the rate capability became worse for the cell using aged electrodes, especially at the negative electrode side.

These results are essentially consistent with those reported by Kötz et al. [21]. That is, the degradation processes depend on the electrolyte solvent, and those occurring at the positive and negative electrodes are respectively responsible for the capacitance decreasing phenomena during the cycles repeated in the acetonitrile- and carbonate-based electrolytes. We also observed no significant differences in the degradation behavior between PC and EC+DMC solvents for the electrolyte.

5. 3. 2. Influences of the electrolyte salt

Influences of the electrolytic salt (cation) on the degradation behavior of EDLC were investigated by comparing the cycling performances of the cells using $TEABF_4$ and $LiBF_4$ as the electrolytic salts dissolved in PC (1 mol dm^{-3}). The charge-discharge curves of the cells under high voltage conditions are shown in Fig. 5.5, for their first cycle. The observed voltage profiles were almost ideal for both cells using $TEABF_4$ and $LiBF_4$ salts when the operation voltage was lower than 3.0 V. However, the voltage stagnation (plateau) appears at around 3.2 V or above, which implies some faradaic process occurring at this voltage region. This voltage duration was more significantly observed for the cell using $LiBF_4$. Variations in the specific capacitance with the cycle number are shown in Fig. 5.6, where each specific capacitance was determined from the discharge branch of the voltage profile, according to eq. (5.3). The capacitance retention with cycle repeated was generally better in $TEABF_4$/PC than in $LiBF_4$/PC. Among the experiments, the difference in the capacitance retention between two electrolytes was clearly noticed for the voltage-limit of 3.5 V (Fig. 5.6c). That is, the capacitance decreasing with the cycling became more significant in the Li salt solution than in the TEA salt solution at higher voltage limit. Fig. 5.7 shows the SEM images of the AC-based electrode surface after the aging tests conducted with the voltage limit of 3.5 V in $LiBF_4$/PC and $TEABF_4$/PC. Some polymeric deposit was observed at the negative electrode surface cycled in the $LiBF_4$ solution (Fig. 5.7b), while much less amounts of deposits were detected at both sides of the electrode cycled in $TEABF_4$/PC (Figs. 5.7c and 5.7d).

The potential profile of each (positive or negative) electrode during the cycling was monitored using a three electrode system equipped with an Ag wire quasi-reference electrode. Fig. 5.8 shows the potential profiles of the positive and negative electrodes together with the variations in the terminal voltage of the cell, where the maximum charging voltage was set at 3.5 V. The rest (starting) potential of each electrode was different between the electrolytic salt. That is, the rest potential was lower in $LiBF_4$/PC by *ca.* 0.3 V than in $TEABF_4$/PC. This potential difference, mainly caused by the difference in the PZC (potential of zero charge) of the carbon surface in the solutions containing Li^+ and TEA^+ [25], would affect the actual values of the potential limit at the

end of charging. Thus, the negative electrode in $LiBF_4$/PC reaches more negative potential than in $TEABF_4$/PC when the cells were commonly charged to 3.5 V of the voltage limit. The result shown in Fig. 5.7b strongly suggests that the decomposition of the electrolyte components to form polymeric deposit is a main cause of the degradation character of the cell using $LiBF_4$/PC electrolyte with the charging voltage limit of 3.5 V. This result on the degradation mode of the cell using PC-based electrolytic solution is well consistent with those observed in the previous work [21]. In order to improve the operation voltage of the cell using PC-based electrolyte solution, we need to find possible way to shift the PZC of the AC-based electrode to slightly positive one.

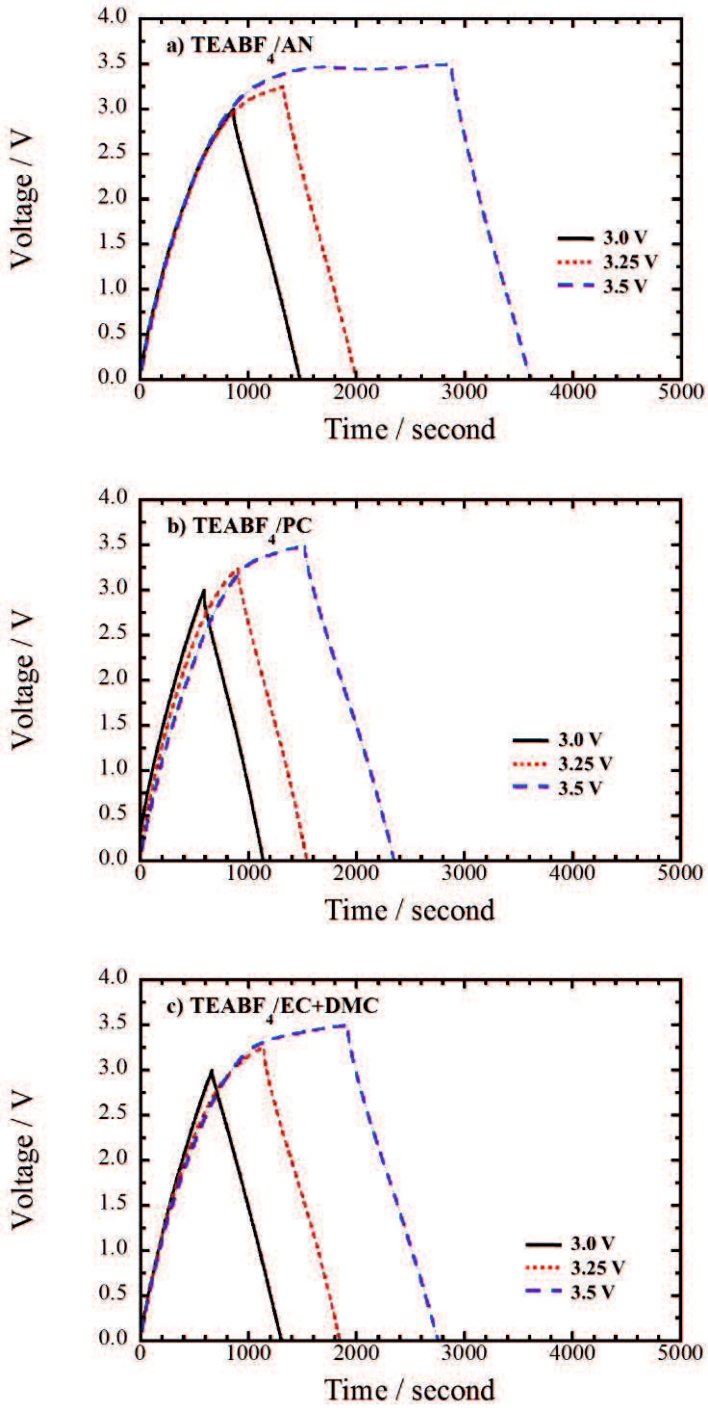

Fig. 5.1 Charge-discharge curves of the cells at 333 K (60 °C) and different cut-off voltages (3.0, 3.25, and 3.5 V).

Electrolyte: 1 mol dm^{-3} $TEBF_4/X$; X = AN (a), PC (b), and EC+DMC (c).

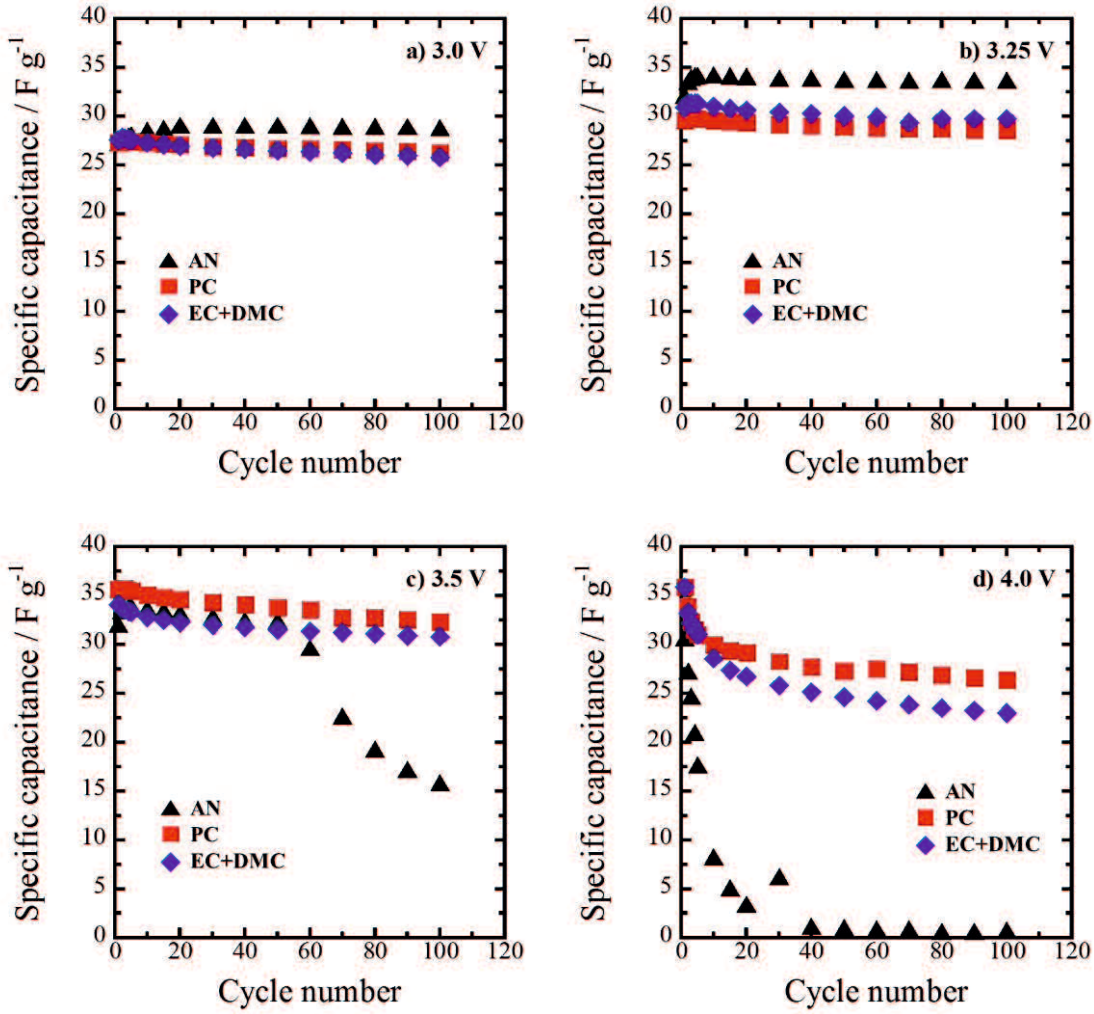

Fig. 5.2 Variations in the specific capacitance of the cells with the charge-discharge cycling at 333 K (60 °C) and different cut-off voltages.

Electrolyte: 1 mol dm^{-3} $TEABF_4$ solutions of AN, PC, and EC+DMC

Cut-off voltage: 3.0 V (a), 3.25 V (b), 3.5 V (c), and 4.0 V (d).

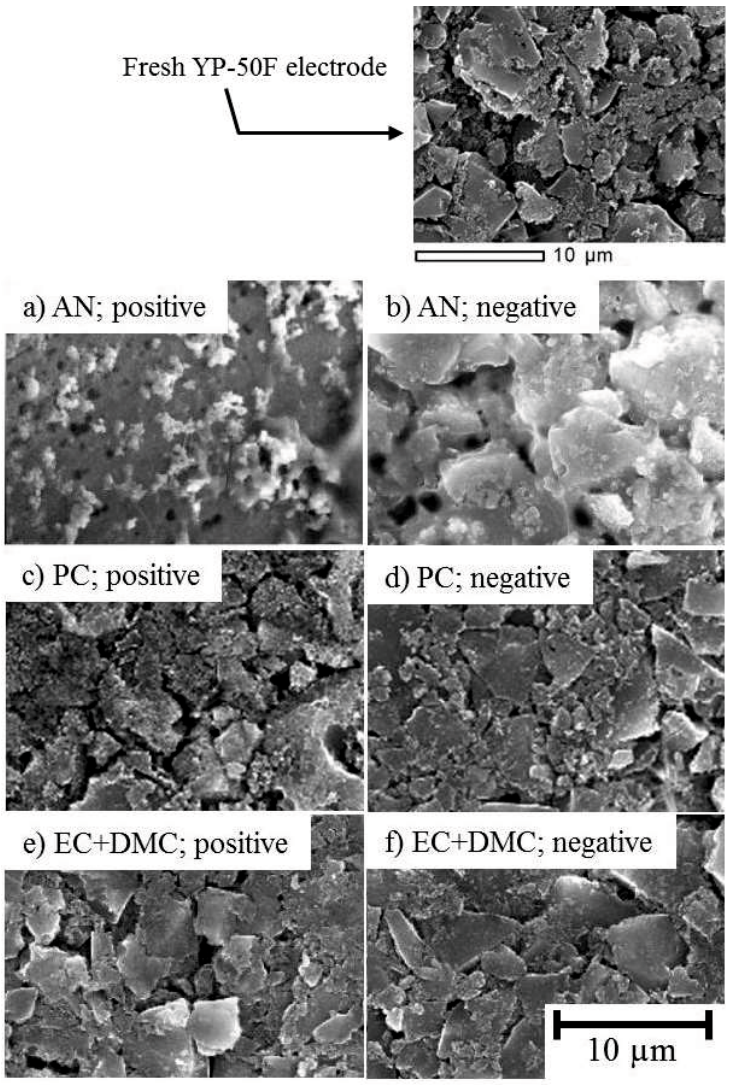

Fig. 5.3 SEM images of aged electrode surfaces after 3.5 V cycling in 1 mol dm^{-3} $TEABF_4$/*X* at 333 K (60 °C).

X = AN; aged positive electrode (a) and aged negative electrode (b),

X = PC; aged positive electrode (c) and aged negative electrode (d),

X = EC+DMC; aged positive electrode (e) and aged negative electrode (f).

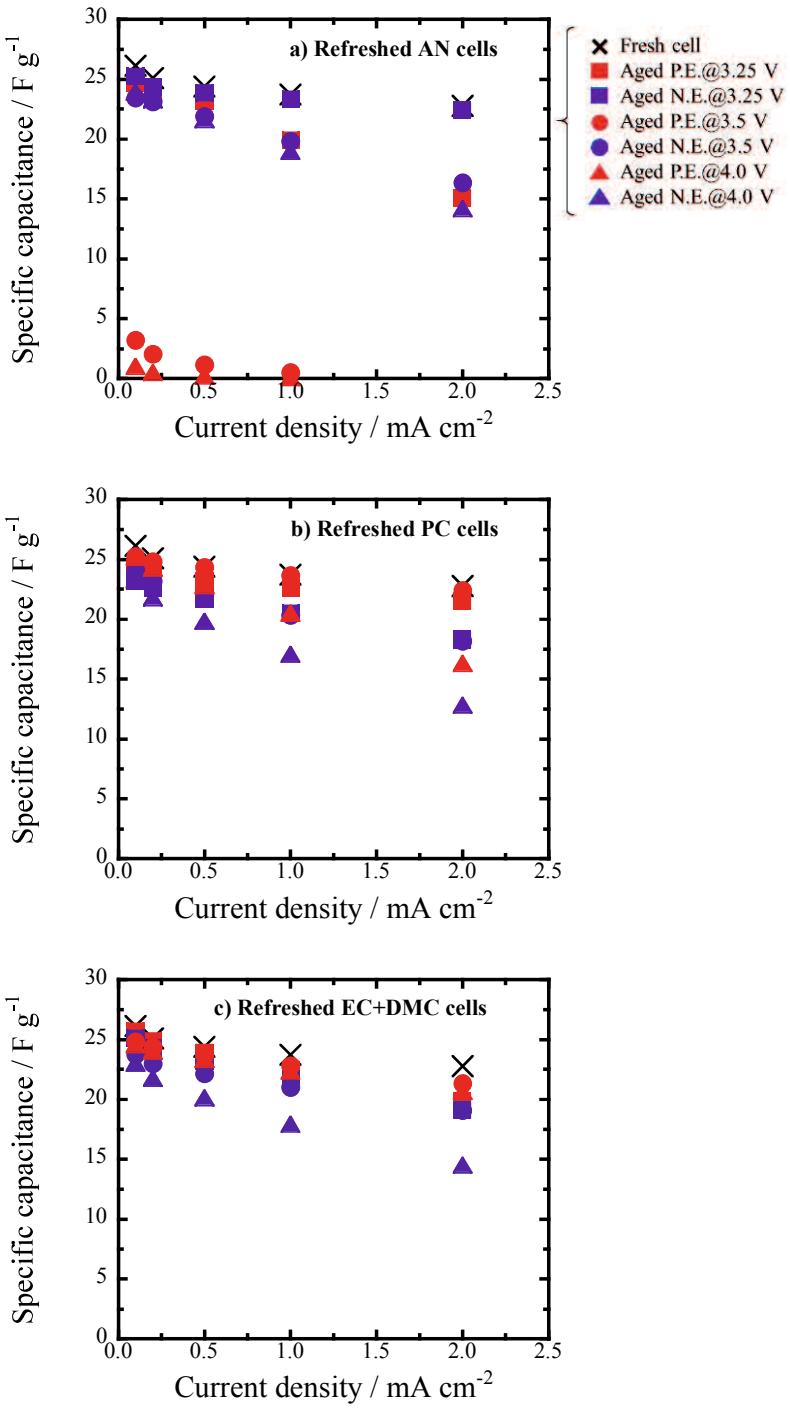

Fig. 5.4 Rate capability of reassembled cells with the electrode aged in each electrolyte and a fresh counter electrode with fresh $TEABF_4$/PC electrolyte. The cycling was done under current density of 2 mA cm^{-2} and voltage range of 0 - 2 V, at 298 K (25 °C).

a) aged in AN, b) aged in PC, c) aged in EC+DMC.

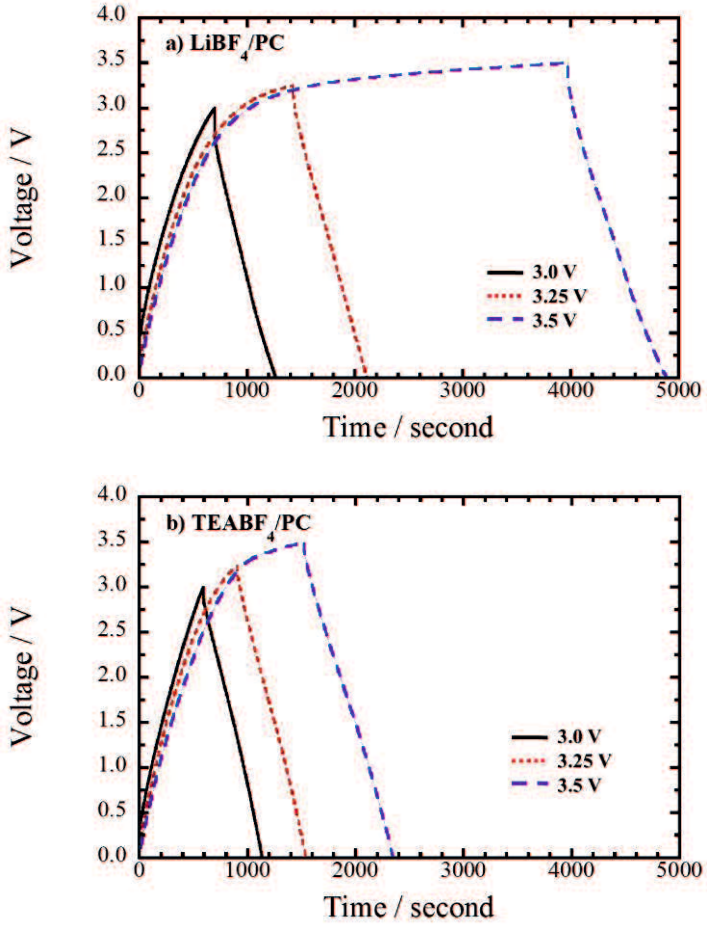

Fig. 5.5 Charge-discharge curves of the cells at 333 K (60 °C) and different cut-off voltage (3.0, 3.25, 3.5 V).

Electrolyte: 1 mol dm^{-3} $LiBF_4$/PC (a) and 1 mol dm^{-3} $TEABF_4$/PC (b).

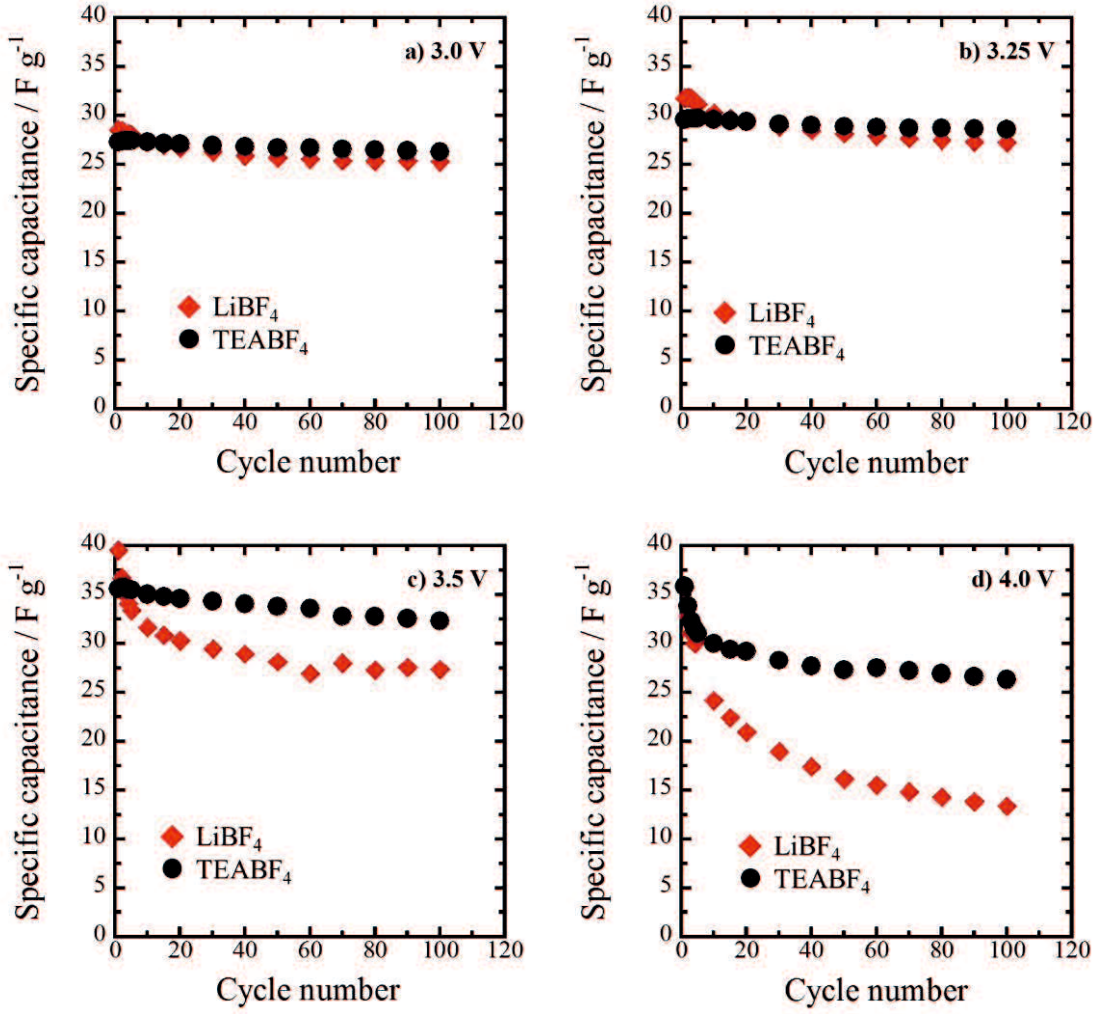

Fig. 5.6 Variations in the specific capacitance of the cells with the charge-discharge cycling at 333 K (60 °C) and different cut-off voltages.
Electrolyte: 1 mol dm^{-3} $LiBF_4$/PC or 1 mol dm^{-3} $TEABF_4$/PC.
Cut-off voltage: 3.0 V (a), 3.25 V (b), 3.5 V (c), and 4.0 V (d).

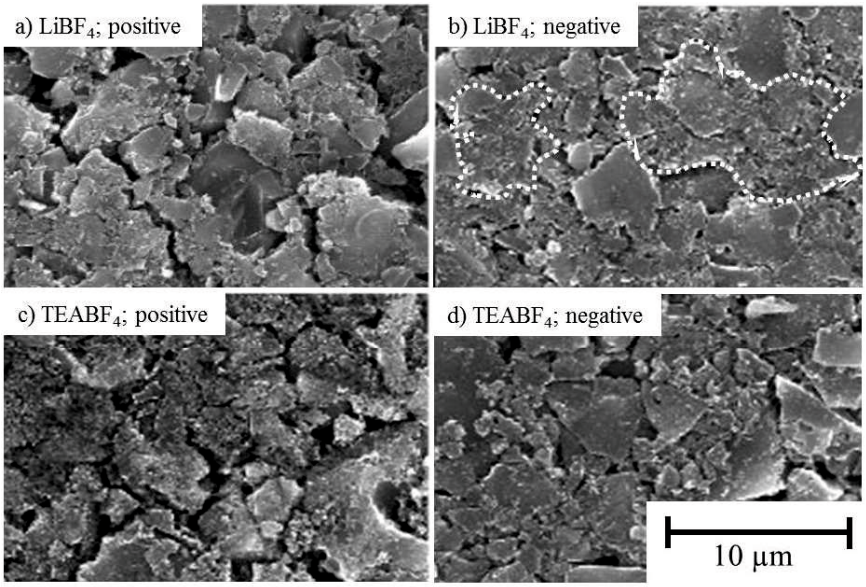

Fig. 5.7 SEM images of aged electrode surfaces after 3.5 V cycling in 1 mol dm^{-3} *Y*/PC at 333 K (60 °C).

Y = $LiBF_4$: aged positive electrode (a) and aged negative electrode (b),

Y = $TEABF_4$: aged positive electrode (c) and aged negative electrode (d).

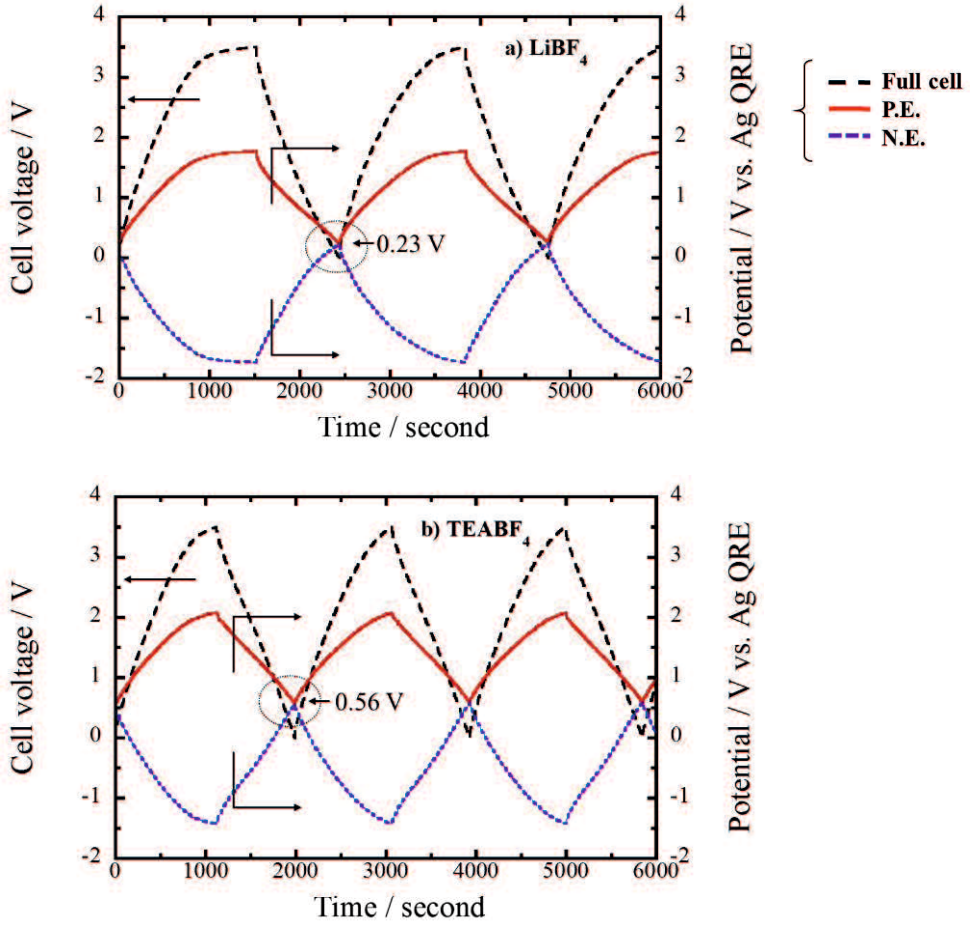

Fig. 5.8 Variations in the cell voltage and each electrode potential during the charge-discharge cycling at 333 K (60 °C) under the cut-off voltage of 3.5 V. Electrolyte: 1 mol dm^{-3} $LiBF_4$/PC (a) and 1 mol dm^{-3} $TEABF_4$/PC (b).

5. 4. Conclusion

Influences of the electrolyte components on the cycle degradation of AC-based EDLC were examined under high-temperature (60 °C) and high-voltage (> 3.5 V) conditions. With respect to the organic solvent, the cell using AN as the electrolyte solvent showed significant degradation at the positive electrode side, comparing with the cells using carbonate solvents, PC and EC+DMC. On the other hand, the cells using carbonate solvents tend to degrade slightly at the negative electrode side. The degradation behavior depended on the electrolyte solvents used due to differences in their electrochemical activity and thermal stability. With respect to the influences of the electrolytic salts on the degradation behavior of EDLC cells, $LiBF_4$ salt lead to more significant decrease in the specific capacitance than $TEABF_4$ at the early stages of the cycling. Changes in positive and negative electrodes were separately monitored during the cycle degradation using a three-electrode cell. The results strongly suggest that the faradaic process at the negative electrode is a main cause of the capacitance decrease with the cycle repeated, especially in the cell using PC solvent. Thus, the significant capacitance loss observed for the cell using $LiBF_4$ salt would be caused by the shift of the electrode potential to more negative one than that observed in the $TEABF_4$ solution.

5. 5. Reference

[1] D. Qu and H. Shi, *Journal of Power Sources*, **74**, 99 (1998).

[2] E. Frackowiak and F. Béguin, *Carbon*, **39**, 937 (2001).

[3] F. Béguin, V. Presser, A. Balducci, and E. Frackowiak, *Advanced Material*, **26**, 2219 (2014).

[4] P. Simon and A. F. Burke, *Interface*, **17**, 38 (2008).

[5] M. Arulepp, L. Permann, J. Leis, A. Perkson, K, Rumma, A. Janes and E. Lust, *Journal of Power Sources*, **133**, 320 (2004).

[6] O. Barbieri, M. Hahn, A. Herzog and R. Kötz, *Carbon*, **43**, 1303 (2005).

[7] Q. Abbas, D. Pajak, E. Frąckowiak and F. Béguin, *Electrochimica Acta*, **140**, 132 (2014).

[8] P. Simon and Y. Gogotsi, *Accounts of chemical research*, **46**, 1094 (2013).

[9] Q. Yang, Z. Lu, J. Liu, X. Lei, Z. Chang, L. Luo, X. Sun, *Advanced Materials*, **23**, 351 (2013).

[10] W. Sugimoto, H. Iwata, Y. Murakami and Y. Takasu, *Journal of Elecrochemcal Society*, **151**, A1181 (2004).

[11] A. Rudge, J. Davey, I. Raistrick, and S. Gottesfeld, *Journal of Power Sources*, **47**, 89 (1994).

[12] G.A. Snook, P. Kao and A. S. Best, *Journal of Power Sources*, **196**, 1 (2011).

[13] S. Ishimoto, Y. Asakawa, M. Shinya and K. Naoi, *Journal of The Electrochemical Society*, **156**, A563 (2009).

[14] K. Chiba, T. Ueda, Y. Yamaguchi, Y. Oki, F. Shimodate and K. Naoi, *Journal of The Electrochemical Society*, **158**, A872 (2011).

[15] P.W. Ruch, D. Cericola, A. Foelske-Schnitz, R. Kötz and A. Wokaun, *Electrochimica Acta*, **55**, 4412 (2010).

[16] M.M. Hantel, D. Weingarth and R. Kötz, *Carbon*, **69**, 275 (2014).

[17] D. Cericola, P. W. Ruch, A. Foelske-Schmitz, D. Weingrath and R. Kötz, *International Journal of Electrochemical Science*, **6**, 988 (2011).

[18] M. Tokita, M. Egashira, N. Yoshimoto, and M. Morita, *Electrochemistry*, **80**, 752 (2012).

[19] M. Tokita, M. Egashira, N. Yoshimoto, and M. Morita, *Electrochemistry*, **81**, 804 (2013).

[20] A.M. Bittner, M. Zhu, Y. Yang, H.F. Waibel, M. Konuma, U. Starke and C.J. Weber, *Journal of Power Sources*, **203**, 262 (2012).

[21] P.W. Ruch, D. Cericola, A. Foelske and R. Kötz, *Electrochimica Acta*, **55**, 2352 (2010).

[22] S. Pohlmann, B. Lobato, T.A. Centeno and A. Balducci, *Physical Chemistry Chemical Physics*, **15**, 17287 (2013).

[23] T. Ohta, I.-T. Kim, M. Egashira, N. Yoshimoto and M. Morita, *J. Power Sources* **198**, 408 (2012).

[24] M. Morita, R. Arizono, N. Yoshimoto and M. Egashira, *J. Appl. Electrochem.* **44**, 447 (2014).

[25] I. T. Kim, M. Egashira, N. Yoshimoto and M. Morita, *Electrochim. Acta*, **56**, 7319 (2011).

Chapter 6.

General Conclusion and Summary

Abstract

6. Conclusion

EDLC has many attractive properties as an energy storage device that reveals much higher energy density than conventional capacitors, much higher power density than common secondary (rechargeable) batteries, and extremely long cycle life (~100,000 cycles), owing to its energy storage mechanism. However, specific energy (Wh kg^{-1}) or energy density (Wh m^{-3}) of EDLC is generally much lower than those of rechargeable batteries in which faradaic processes are utilized. In order to increase the storable electric energy, enhancing the specific capacitance and/or extending the operation cell voltage are practically efficient to realize higher-performance EDLCs. Typical EDLC cells are constructed by activated carbon (AC) as the main active electrode materials due to their high specific surface area (~2000 m^2 g^{-1}), and organic electrolyte solutions, eg., tetraethylammonium tetrafluoroborate ($TEABF_4$) dissolved in propylene carbonate (PC) with around 1 mol dm^{-3} concentration. Activated carbon for the electrode material has a complex pore structure on the surface, and there are many non-contributed parts to the capacitance. Furthermore, for such the electrode/electrolyte system, cycling stability becomes lowered when the cycles are done under higher voltage than ca. 2.7 V, especially under elevated temperature conditions.

In this work, to increase the energy density (or specific energy) of EDLC, carbon materials with controlled nano-structures have been prepared, in which efficient capacitance enhancement would be expected, and the degradation phenomena under the high-voltage cycling were examined from the viewpoints of both contributions of nano-structure of electrode material and the electrolyte components. The results obtained are summarized as follows:

In Chapter 2, porous carbon with a uniform nano-structure was newly prepared, and then composites were made with fibrous nano-carbons with highly conductive networks to obtain higher capacitance and power performances. The uniform mesopore created by the carbonization of *R-F* gel containing a triblock copolymer surfactant can be reproduced on nano-carbon substrate to some extent by selecting such conditions as carbonization atmosphere, the composition of the substances (mixing ratio of the mesoporous carbon (MC) precursor and the substrate), and the kind of substrate. In the present trial, the

composite carbons with the surface area of 100 ~ 250 m^2 g^{-1}, and the ratio of controlled mesopore volume to total pore volume reaches *ca.* 50 % at the best. The flow condition of argon on carbonization process and the kind of substrate influences on the pore structure of the composite. The performance of test double-layer capacitor cells including the VGCF/MC electrodes in symmetric configuration depends on the pore structure of the composite electrode. That is, the mesopore of 3.8 nm on the composite electrode provides similar double-layer capacitance to the smooth surface of the CNT electrode. In the best case of the present study, the VGCF/MC composite provides rather comparable cell performance compared with the CNT cell.

In Chapter 3, influences of the surface structure of carbon material on the degradation behavior of EDLC were investigated by using fibrous nano-carbon materials. VGCF is well known as fibrous nano-carbon with exposed graphene surface. Here alternative fibrous nano-carbon with amorphous carbon structure has newly been prepared by the carbonization of cellulose fiber derived from biomass (BCNF), and its electrochemical behavior, in particular concerning on aging, is compared with VGCF. BCNF has amorphous structure and specific surface area of 28 m^2 g^{-1}, and oxygen-containing functional groups. The influence of graphitic structure of carbon electrode on the aging process can be elucidated by comparing the aging behavior of the cells consisting of BCNF and VGCF. Amorphous BCNF provides similar capacitance per unit surface area to that of VGCF, despite of different surface structure. On accelerating aging test using constant voltage of 3.5 V and high temperature, BCNF provides the degradation in the cell capacitance because of the decrease in the effective surface area by deposition of decomposition product. In contrast, VGCF provides the increase of capacitance by surface etching.

In Chapter 4, influences of the pore structure of high surface area carbon electrode were focused on the aging behavior of EDLC, especially for the capacitance and rate capability. The reproducibility of porous carbons with various nanostructures from α-cyclodextrin has been assessed under different heating rates, and their electrode properties have been compared with each other, *ie.* α-cyclodextrin-derived carbons (CyDCs). Carbon materials having different nano-structures were obtained by simple carbonization of α-cyclodextrin with different heating conditions: CyDC10 (heating rate being 10 K min^{-1}) has larger

particle size with significant micropores and CyDC50 (heating rate being 50 K min^{-1}) has smaller particle size with higher ratio of mesopore volume. The rate capability of the double-layer capacitance depended on the nano-structures of CyDCs. The accelerated aging tests using server cycling conditions (constant-voltage charging at 3.5V for 5 h at 333 K) showed that CyDC50 having higher ratio of mesopore volume leads to the degradation of the cell capacitance significantly, compared with that of CyDC10. The AC impedance results after the accelerated aging tests suggest that the differences in the decomposition process of the electrolyte component are responsible for such degradation process.

In Chapter 5, influences of the electrolyte components on the cycle degradation of AC-based EDLC were examined under high-temperature and high-voltage conditions. With respect to the organic solvent, the cell using AN as the electrolyte solvent showed significant degradation at the positive electrode side, comparing with the cells using carbonate solvents, PC and EC+DMC. On the other hand, the cells using carbonate solvents tend to degrade slightly at the negative electrode side. The degradation behavior depended on the electrolyte solvents used due to differences in their electrochemical activity and thermal stability. With respect to the influences of the electrolytic salts on the degradation behavior of EDLC cells, $LiBF_4$ salt lead to more significant decrease in the specific capacitance than $TEABF_4$ at the early stages of the cycling. Changes in positive and negative electrodes were separately monitored during the cycle degradation using a 3-electrode cell. The results strongly suggest that the faradaic process at the negative electrode is a main cause of the capacitance decrease with the cycle repeated, especially in the cell using PC solvent. Thus, the significant capacitance loss observed for the cell using $LiBF_4$ salt would be caused by the shift of the electrode potential to more negative one than that observed in the $TEABF_4$ solution.

In summary, nano-structure of the carbon materials affected not only the main performances (specific capacitance, rate capability, etc.) but also the degradation processes (aging behavior) of EDLC devices. The electrolyte components also influenced the degradation behavior. Cells using alkyl carbonate-based electrolytes could be expected for designing more stable cells under the high-voltage and high-temperature conditions using electrolyte salts with proper compatibility with the carbon surface.

Acknowledgement

私が山口大学に入学してから 10 年、研究室に配属されてからは 6 年が過ぎ、ついに卒業を迎えることが出来ました。

学部生の頃は座学があまり好きではなく、大変不真面目な学生でしたので、山口大学の応用化学科の先生方には多大なご迷惑をお掛けしたと思います。

研究室に配属後は、江頭 港准教授 (現 日本大学) の下で研究に励み、数多くの学会発表の機会を与えていただきました。江頭先生は学生との会話を大事にされ、私にも研究以外のことでもいろいろな話をしてくださっていたのを今でも鮮明に覚えています。また、就職か博士後期課程に進学か悩んでいるときに色々と相談に乗っていただき、その結果、進学を決心することが出来ました。その後、江頭先生が日本大学に異動されることを知ったときは大変ショックを受けたことを覚えています。それからは、同研究室の森田 昌行教授の下で研究することになりました。これまで“電子化学研究室”は森田先生と江頭先生、そして分子反応研究室の吉本 信子准教授と共に研究を行っていました。森田先生は、これまでも中間報告、学会発表などで色々とアドバイスを下さっていましたが、急に博士課程の学生を面倒見ないといけない環境になったにもかかわらず、私を温かく迎え入れてくれました。今年度のモンペリエ (フランス) での学会の時には学生一人の私を気にかけて下さり、有名な先生方に挨拶する機会や食事に連れて行って頂き、改めて森田先生の温かみを感じ、これまで森田先生の下で研究することが出来て本当によかったと感じました。時には厳しい意見をいただいたこともありましたが、今日こうしてこの博士論文をまとめ上げることが出来たのは森田先生の多大なご助力があってこそだと思います。その間、日本大学に行かれましても私を気遣って下さった江頭先生、まるで母親のように私を気にかけてくださいました吉本先生、昨年度から新しく本研究室にいらっしゃった兄貴肌の藤井 健太准教授のお力添えもありました。また、これまで大きなストレスに悩まされることなくここまで来れたのは多くの後輩が私に明るく接してくれ、食事、飲み会などに付き合ってくれたからこそだと思っております。本当にこの“電子化学研究室”で学んでこれたことを誇りに思います。

また、長い間学生の私を見守って下さった両親には言葉では感謝しきれないのでこれから社会人として精一杯の恩返しをしていきたいと思います。

最後に、本論文に関して多大なお時間をいただきまして審査してくださった審査員の森田先生、比嘉 充教授、中山 雅晴教授、吉本先生、藤井先生に厚くお礼を申し上げます。